Fundamental Research on Gear Lubrication

By

Tokio SASAKI*, Kenjiro OKAMURA* and Tadataka KONISHI*

(Received March 30, 1966)

In this paper, the fundamental characteristics of gear lubrication were synthetically clarified, and the oil-film formation between mating gear-teeth was investigated, taking into consideration the dynamic performance of gear-teeth.

Using roller and gear testing equipments, the fundamental lubrication characteristics were measured under various driving conditions, and the lubrication characteristic was classified into three regions. The correlation between both lubrication characteristics of rollers and gears was investigated referring to the experimental results, and it is deduced that the analysis of the dynamic phenomena owing to gear mating is very important.

The transient characteristics of oil-film due to the gear-mesh were theoretically analyzed, and the transient performance of oil-film was experimentally measured using special models of rollers. The dynamic lubrication theory was applied to the practical gears in consideration of the tooth deflection, and the variation of oil-film thickness was measured through over-all range of a gear-tooth mesh using a special test gears. From these results, the principle of oil-film formation in gears were discussed.

Introduction

With an increasing use of various kinds of gears under severe conditions, the effect of lubrication has become a very important problem. The use of rationally lubricated gears is possible only by adopting the well-founded lubricating condition and lubricating method, and various damages and wears of gear-tooth will be preventable. Therefore, the study on the mechanism of gear lubrication is a fundamental problem.

The purpose of this research is to investigate the mechanism of gear lubrication by clarifying the lubrication characteristics and the principle of oil-film formation on mating gear-tooth surfaces.

Part I. Fundamental Characteristics of Gear Lubrication

1. Introduction

In order to clarify the fundamental characteristics of gear lubrication,

---

* Department of Precision Mechanics.

this experimental investigation was carried out using roller and gear testing equipments with which the testing conditions were changed to a great extent, corresponding to the actual driving conditions of practical gears. The investigations, referring to the experimental results, were concerned with the correlation between both lubrication characteristics of gears and rollers, the application of rollers to the experimental study of gears and the limit of the application.

2. Relation between the Mechanism of Friction and the Relative Motion on Gear-tooth Surface

The oil-film pressure between contact surfaces is generated by a relative sliding motion and a relative rolling motion. At the pitch point on mating gear-tooth surfaces, the oil-film is generated only by a relative rolling motion, and on the other mating tooth surfaces it is generated by a relative sliding motion with rolling. In this case, factors influencing the oil-film formation are the relative radius of curvature, the sliding velocity, the rolling velocity and the specific sliding.

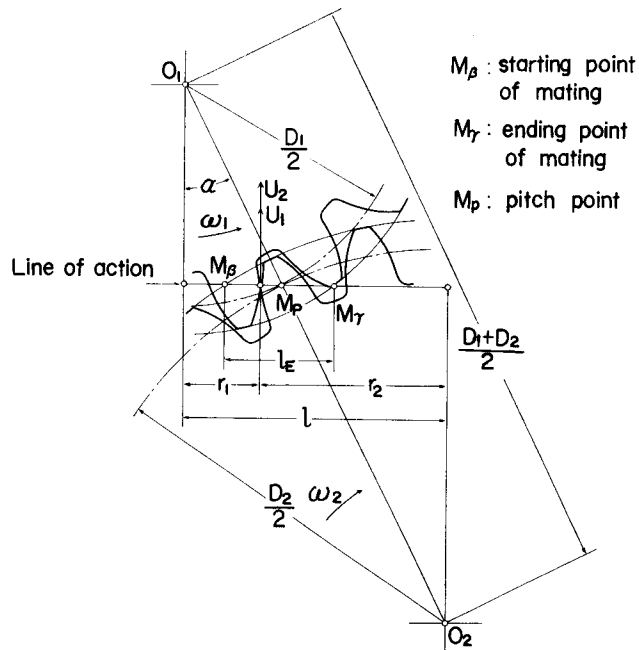From Fig. 1, the relative radius of curvature r is found as follows:

Fig. 1. A pair of mating spur gears.

$$r \equiv \frac{r_1 r_2}{r_1 + r_2} = \frac{1}{2} D_1 X (1-X)(1+i) \sin \alpha \qquad (1)$$

where α: pressure angle, $i = D_2/D_1$: gear ratio

$$X = r_1/l, \quad (1 \geqq X \geqq 0)$$

The starting point of mating X_β and the ending point of mating X_γ are obtained as follows:

$$\left. \begin{array}{l} X_\beta = 1 - \dfrac{\sqrt{(iD_1 + 2C)^2 - (iD_1 \cos \alpha)^2}}{D_1(1+i) \sin \alpha} \\[2ex] X_\gamma = \dfrac{\sqrt{(D_1 + 2C)^2 - (D_1 \cos \alpha)^2}}{D_1(1+i) \sin \alpha} \end{array} \right\} \qquad (2)$$

where C: addendum length

The maximum relative radius of curvature r_{max} is only about 0.24 m, even in the case of such a very large gear as follows: $D_1 = 5000$ mm, $i = 5$, $\alpha = 20°$. From this result, it is clear that the relative radius of curvature on the gear-tooth surfaces is not to be compared with that of a plain bearing.

The sliding velocity U_s and the rolling velocity U are obtained as follows:

$$U_s \equiv U_1 - U_2 = \frac{1}{2} \omega_1 D_1 \{(1+i)X - 1\} \frac{1+i}{i} \sin \alpha \qquad (3)$$

$$U \equiv \frac{U_1 + U_2}{2} = \frac{1}{4} \omega_1 D_1 \{1 - (1-i)X\} \frac{1+i}{i} \sin \alpha \qquad (4)$$

where ω_1: angular velocity of driving shaft

The specific sliding s is defined as follows:

$$s \equiv \frac{U_s}{U} = 2 \left\{ \frac{(i+1)X - 1}{(i-1)X + 1} \right\}. \qquad (5)$$

As to basis of discussions of experimental results, we take the Martin's theory[1] under the Reynolds' condition. For the oil-film formed between contact surfaces of rolling disks as shown in Fig. 2, the Martin's theory gives following relations:

Maximum pressure

$$p_{max} = 0.195 \frac{P}{r} \sqrt{\frac{P}{\eta U}} \qquad (6)$$

Minimum oil-film thickness $\qquad h_0 = 4.896 \frac{\eta U}{P} r \qquad (7)$
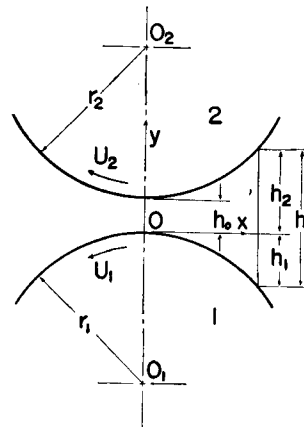
Fig. 2. Contact of rolling disks between which oil-film is formed.

Friction coefficient $$f = 2.079\sqrt{\frac{\eta U}{P}}(1+0.619s) \qquad (8)$$

where　P: contact load or load capacity of oil-film per unit width

　　　　η : absolute viscosity of lubricant

3.　Lubrication Characteristics on the Contact Surface of Rolling Disks with Sliding

3.1.　Experimental Equipment and Procedure

The experimental equipment used is shown in Fig. 3. It is constructed of a disks-machine, measuring instruments of frictional torque and electrical resistance between two disks running in contact, a lubricant supply unit and a measuring apparatus for lubricant temperature.
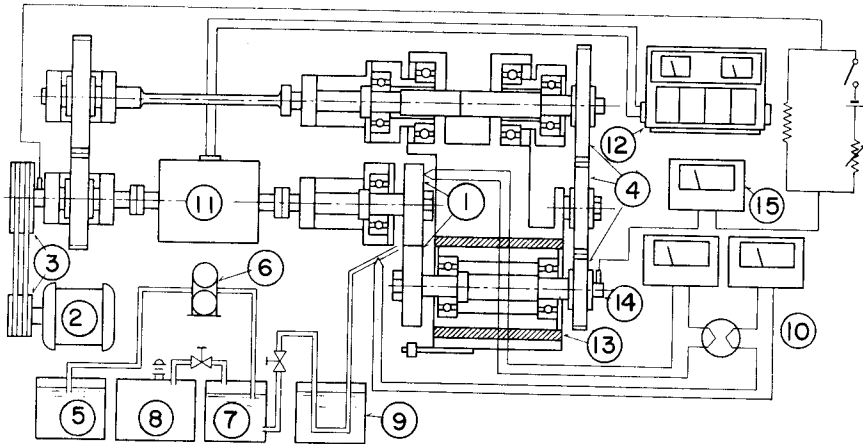

Fig. 3.　Arrangement of experimental equipment.

In Fig. 3, testing disks are shown as ①. For the disk material, Cr steel with hardness $H_RC = 12$ or 59 is used. The contact surface of disk is super-finished to $H_{max} = 0.1\mu$ without the test of the effect of roughness. The disks machine is driven by the electric motor ②, and the rolling velocity U is varied by exchanging the V–pulley ③. The specific sliding s is varied by exchange of the gear train ④. Fine adjustment of specific sliding is made by variation in disk diameter. The gear pump ⑥ feeds the lubricant (straight turbin oil ♯90 or engine oil ♯50) to the pressurized tank ⑦ from the oil reservoir ⑤. The oil viscosity η is controlled by the heating and cooling bath ⑨, and the oil is supplied to testing disks. The temperature of oil and testing disks is measured by the thermocouple pyrometer ⑩. The frictional torque T_f is picked up by the torque-meter ⑪ with a strain gages bridge,

and is measured by the strain meter ⑫. In this case, the friction loss by the ball-bearings is calibrated previously and deducted from the measuring results. The electrical resistance of oil-film R between two disks is measured by the ammeter ⑮. The shaft of the upper disk is electrically insulated from the lower disk using the cylinder ⑬ and the idle gear in the gear train ④ which are made of bakelite. The measuring apparatus of the relation between the resistance R and the oil-film thickness h_0 is constructed of a fine adjuster of clearance between two disks by an application of elastic deflection of a beam and a differential transformer type micrometer. Using this apparatus, the clearance can be measured more accurately than 1μ.

The characteristics of the testing equipment are as follows:

Disk diameter	$D=40$ to 60 mm
Disk width	$b=10$ mm
Rotating speed	$N=100$ to 3580 rpm for the upper shaft
	600 to 3580 rpm for the lower shaft
Rolling velocity	$U=1$ to 12 m/s
Specific sliding	$s=0$ to 1.61
Contact load	$P=20$ to 600 kg/cm

3.2. Experimental Results

(1) Effect of contact load P

Fig. 4 gives some examples of experimental results tested with various loads P. It is found from this figure that the frictional torque T_f increases with an increase in P, and the inclination of curves is almost constant on the logarithmic charts except the case of $s=0$.

(2) Effect of rolling velocity U

Fig. 5 shows the relation between frictional torque T_f and rolling velocity U. Every curve shows a diminishing tendency. This fact indicates that the oil-film is easily generated with an increase in U. But at higher viscosity, the inclination of curves and the value of T_f are smaller. This seems to be the effect of U in the fluid lubrication.

(3) Effect of dimensionless parameter $\eta U/P$

If the lubrication characteristic is in the fluid lubrication, the lubricating performance at the disks machine will be regulated by dimensionless parameter $\eta U/P$ as shown in Eqs. (7) and (8). Fig. 6 shows the relation between friction coefficient f and $\eta U/P$. The solid curves show the results obtained
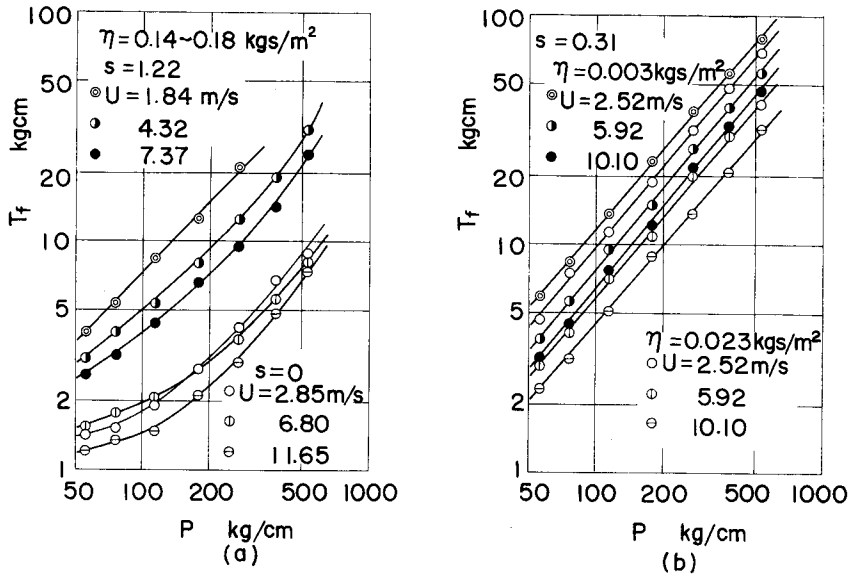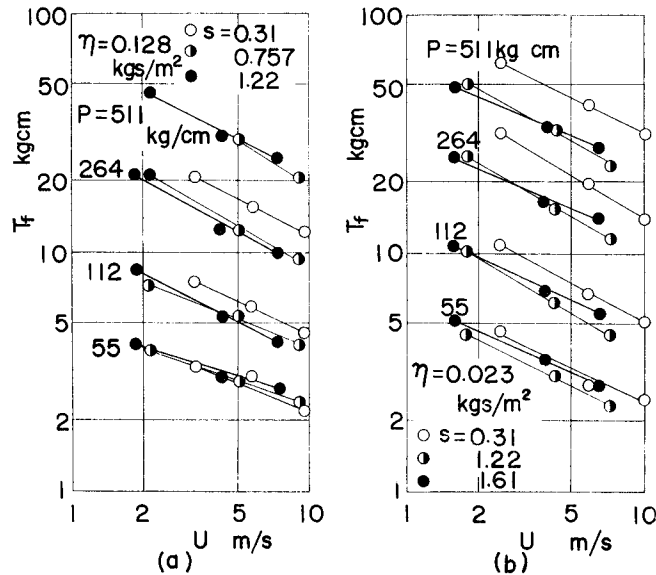
Fig. 4. Frictional torque versus contact load.

Fig. 5. Frictional torque versus rolling velocity.

from the experiment with various contact load P under constant s, U and η. The dotted curves show the theoretical relations from Eq. (8). Almost all the solid curves decrease with an increase in $\eta U/P$. This shows that the most part of the tests were carried out in the range of semi-fluid lubrication.
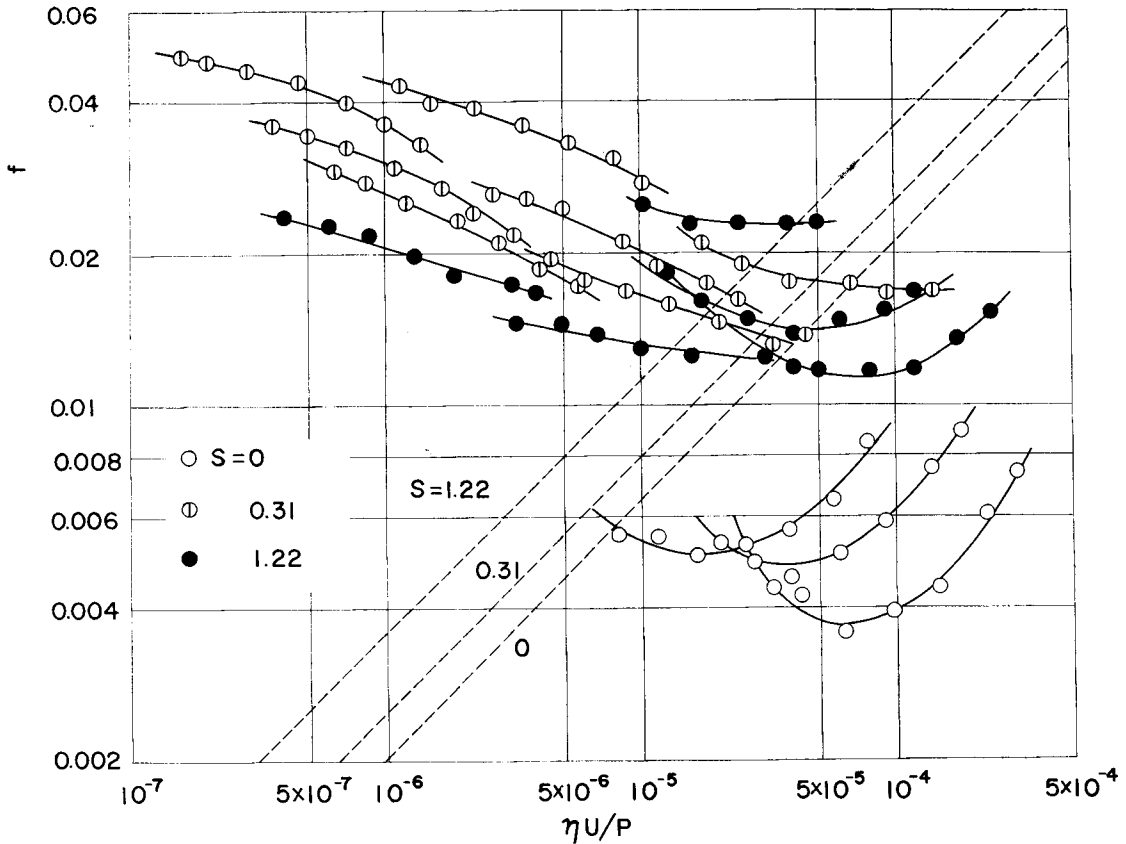
Fig. 6. Friction coefficient versus dimensionless parameter $\eta U/P$.

The minimum value of f is found in the neighbourhood of $\eta U/P=5\times10^{-5}$, and the value of f seems to be almost constant in the range of $\eta U/P<5\times10^{-7}$. Therefore, the lubrication characteristic is classified into three regions by $\eta U/P$.

Boundary lubrication $\qquad\qquad\qquad \eta U/P<5\times10^{-7}$

Semi-fluid lubrication $\qquad\quad 5\times10^{-7}<\eta U/P<5\times10^{-5}$

Fluid lubrication $\qquad\qquad\quad 5\times10^{-5}<\eta U/P$

In Fig. 6, the experimental value of f in fluid luburication is smaller than the theoretical value, and especially a great difference is found in the case of pure rolling. There are, of course, many factors which have not been taken into account in the derivation of the theorectical equations. Namely, Eq. (7) is induced without considerations about the elastic deformation of disks, the width effect of disks and the variation of oil viscosity due to the variation of oil pressure and temperature on the contact surface. Moreover,

the values of η and P used in the calculation of $\eta U/P$ will be different from the actual values owing to the measurement error of oil temperature, roughness of contact surfaces and etc. When $\eta U/P$ is equal to 1×10^{-4}, the theoretical value of oil-film thickness h_0 obtained from Eq. (7) is 7.3μ, but the actual value seems to be smaller from the measured results of electrical resistance.

(4) Effect of specific sliding s

The effect of specific sliding s upon friction coefficient f and oil-film thickness h_0 is shown in Fig. 7. The testing conditions are shown as follows:
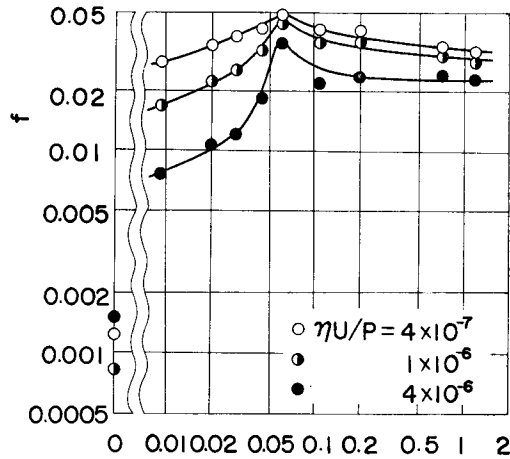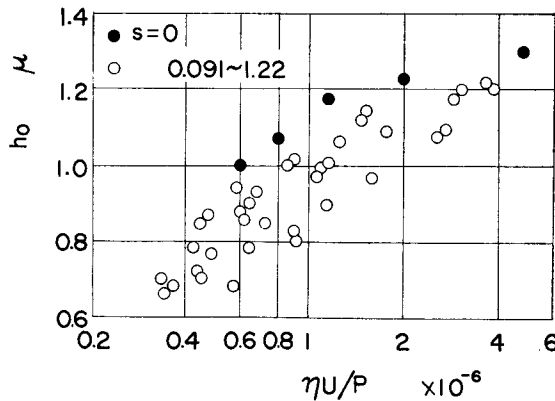
Fig. 7. Effect of specific sliding upon friction coefficient and oil-film thickness.

$$P=55 \text{ to } 420 \text{ kg/cm}, \quad \eta=0.004 \text{ to } 0.006 \text{ kg·s/m}^2, \quad U=4 \text{ m/s}$$

As shown in Fig. 7(a), every curve shows the maximum value of f at $s=0.06$. The cause that the maximum value of f is obtained at a constant value of s is explained as follows: the shearing action in oil-film is accelerated owing to an increment of s, and consequently f becomes larger. By the way the oil-film temperature at contact surface is raised, owing to an increment of shearing action of oil-film. As the result of this action, f becomes smaller. When the value of s is small, the former action is large, and when the value of s becomes larger, the latter action increases. To summarize, as the resultant effect of both actions, we can find the maximum value of f at a constant value of s.

Considering this result in conformity with gear, the corresponding point of $s=0.06$ on gear-tooth surface is the vicinity of pitch point. Then, the maximum friction is obtained on the surface in the vicinity of pitch point. Moreover, the fact that the pitting occurs in the vicinity of pitch point on the deddendum side of gear-tooth is stated in many reports. Accordingly, it may be thought that the effect of the maximum friction at $s=0.06$ is one of the reasons causing the pitting on gear-tooth surface.

Fig. 7(b) shows the results of measurement on oil-film thickness. The data points disperse, but the effect of specific sliding cannot be found distinctly excepting that the value of oil-film thickness is rather greater in the case of pure rolling. Then, it may be recognized experimentally that the specific sliding has little influence upon the oil-film thickness. This result is qualitatively in agreement with the theoretical result obtained from Eq. (7).

(5) Effect of relative radius of curvature r

The effect of relative radius of curvature r on the lubrication characteristic was measured in the following driving conditions:

$$P=55 \text{ to } 420 \text{ kg/cm}, \quad \eta=0.0037 \text{ kg·s/m}^2, \quad U=4 \text{ m/s}, \quad s=0.3$$

Experimentally, the relative radius of curvature r has no influence upon the friction coefficient. It can be recognized theoretically, that is, r is not contained in Eq. (8).

In Fig. 8, it is shown that the minimum oil-film thickness h_0 is proportional to the relative radius of curvature r and dimensionless parameter $\eta U/P$ in the range of $\eta U/P > 1 \times 10^{-6}$ which corresponds to the region of semi-fluid lubrication. This is in good agreement with the theoretical relation shown
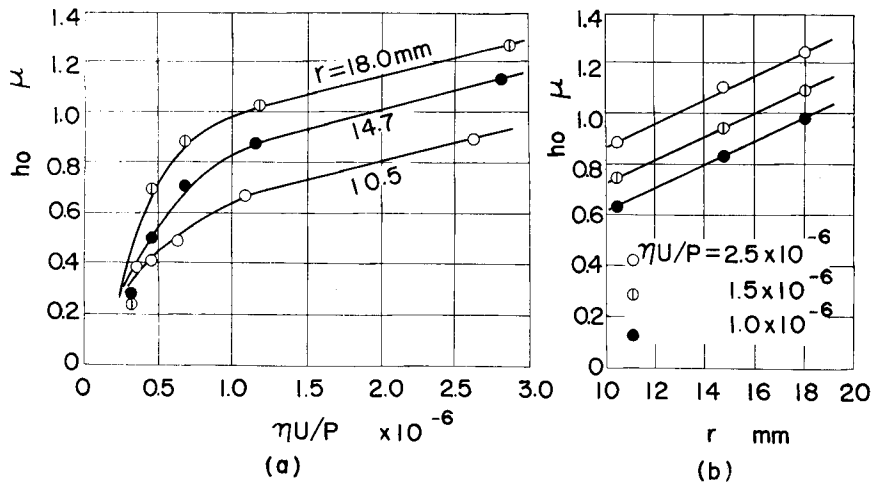
Fig. 8. Effect of relative radius of curvature upon oil-film thickness.

in Eq. (7). But in the range of $\eta U/P < 5 \times 10^{-7}$ corresponding to the region of boundary lubrication, the oil-film thickness has no connection with r. Accordingly, it may be said that the oil-film in the region of semi-fluid lubrication is formed by the same principle as in the region of fluid lubrication, but the generating mechanism of oil-film in the region of boundary lubrication is different.

(6) Effect of surface roughness H_{max}

The roughness of gear-tooth surface is a passable value, and it will have great influence upon the lubrication characteristic. In order to investigate the relation between the lubrication characteristic and the contact surface roughness, the following rough surfaces are taken for the initial surface roughness:

$$_0H_{max} = 22 \text{ to } 17\mu, \quad 12 \text{ to } 7\mu, \quad 5 \text{ to } 4\mu.$$

The disk surface which comes in contact with those rough surfaces is super-finished in order to avoid a complicated phenomenon occurring from meshing asperities. The driving conditions are as follows:

$$P = 132 \text{ and } 324 \text{ kg/cm (apparent values)}, \quad U = 9.6 \text{ m/s}$$
$$\eta = 0.0025 \text{ to } 0.0027 \text{ and } 0.16 \text{ to } 0.25 \text{ kg·s/m}^2, \quad s = 0.33$$

The roughness decreases as running time goes on. Fig. 9 shows the total results of the relation between friction coefficient f and H_{max}. Therefore, the data points contain the results with various contact conditions. Some of them are obtained from the contact of triangular asperities and others from the contact of trapezoid asperities. But as shown in the figure, it can
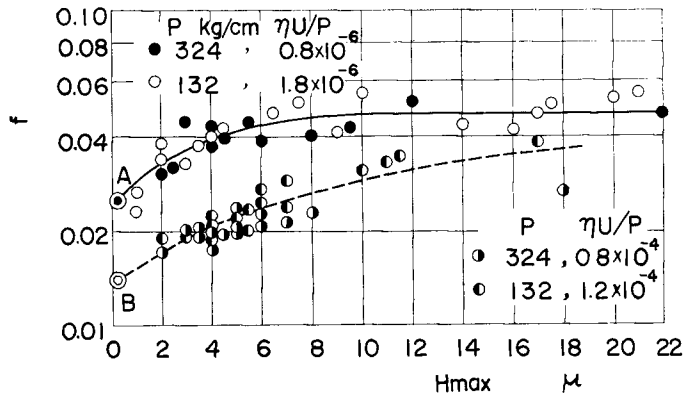
Fig. 9. Friction coefficient versus surface roughness

be seen that the data points can be separated into two curves with regard to the value of $\eta U/P$. When $\eta U/P$ is large, f increases with an increase in H_{max}, but when $\eta U/P$ is small, H_{max} has no influence upon f in the range of $H_{max} > 6\mu$, and the value of f in this range is nearly equal to that obtained from the ideal surface contact in the region of boundary lubrication. In the range of $H_{max} < 6\mu$, f decreases with a decrease in H_{max}. To summarize, it is desirable to use a surface with $H_{max} < 4\mu$ for improving the frictional characteristics of gears.

4. Lubrication Characteristics on the Mating Gear-tooth Surface

4. 1. Experimental Equipment and Procedure

The experimental equipment used is shown in Fig. 10. It is constructed of a gear testing machine, measuring instruments of frictional torque and electrical resistance between mating gears, a lubricant supply unit and a measuring apparatus for oil temperature. The power circulating system is adopted for the gear testing machine.

The electric motor ① drives the test spur gears ③. The angular contact ball bearings of the main shafts ④ and ⑤ are adequately pre-loaded and lubricated with oil mist. The gears are loaded by the springs ⑥, and the torque circulates in the sequence of $A_1A_2B_2B_1A_1$. The lubricating methods for gears is the oil-bath and the oil-jet lubrication. Lubricants used are straight turbine oil ♯90 and engine oil ♯50. The oil temperature is measured by the thermocouple pyrometer ⑦. The frictional torque is picked up by the torque-meter ⑧, and is measured by the strain meter ⑨. The measuring results are compensated for the frictional loss by the ball bearings. The electrical resistance R between mating gears is measured by the ammeter
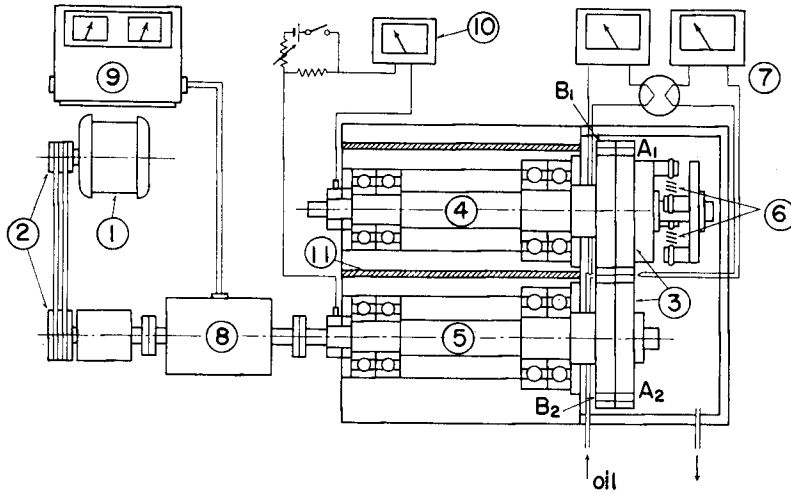
Fig. 10. Arrangement of experimental equipment.

⑩. The shaft ④ is electrically insulated from the other part of the machine with the insulating cylinder ⑪.

The characteristics of the testing machine are as follows:

Center distance of main shafts $d=120$ mm
Rotating speed $N=480$ to 3500 rpm
Contact load $P=20$ to 300 kg/cm
Maximum circulation power $L_{max}=65$ kw

The tooth form of test gears is involute standard gear-tooth of ordinary depth, and gear material used is Ni-Cr steel. The tooth surface is carburized, quenched and ground. The main dimensions of test gears are as follows:

Pressure angle $\alpha=20°$,   Module $m=4$
Contact width $B=10$ mm,   Number of tooth $z=30$
Gear ratio $i=1$,   Specific sliding $s=0$ to 0.95
Relative radius of curvature $r=7.9$ to 10.3 mm

4. 2. Calculation of Friction Coefficient on Gear-tooth Surface

In Fig. 10, two pairs of mating gears are: (A_1, A_2) and (B_1, B_2). There are two cases that one or two pairs of gear-tooth are mating at the same time for (A_1, A_2) and (B_1, B_2). Supposing that the discrepancy between the mating positions for (A_1, A_2) and (B_1, B_2) is equal to the half of the normal pitch l_n as shown in Fig. 11, the number of mating points for all test gears is three or four. Therefore, the frictional torque measured with the testing machine is the total amount under the condition of three or four contact
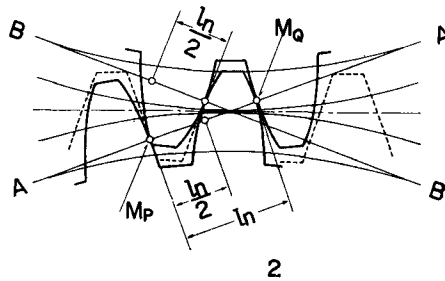
Fig. 11. Positional relation between mating
gear-teeth

points.

The torque T_M measured with the torque-meter is expressed as follows:

$$T_M = T_A + T_B + T_l \qquad (9)$$

where T_A: torque of shaft ⑤ produced by (A_1, A_2) gears

T_B: torque of shaft ⑤ produced by (B_1, B_2) gears

T_l: frictional torque at the bearings between the test gears and
torque-meter

The angular contact ball bearings of main shafts are adequately pre-
loaded, and the amount of increase in friction loss ΔT_l at the bearings due
to the reaction force caused by mated gears was measured by the balance-
beam method. The result was that ΔT_l was negligibly small for the purpose
of measuring the average friction coefficient f_m. Therefore, T_l is nearly
equal to the friction loss due to the pre-load. T_A and T_B are expressed as
follows:

$$T_A = T \mp r_2 F, \quad T_B = -T \pm r_2' F \qquad (10)$$

where $\qquad T$: load torque given

r_2 and r_2': radii of curvature at mating points for A_2 and B_2 gears

F: frictional force acting on mating gear tooth surface
(its direction changes at the pitch point)

The torque due to friction on gear-tooth surfaces T_f is given as follows:

$$T_f = T_M - T_l = \mp r_2 F \pm r_2' F \qquad (11)$$

T_f is positive if this amount is in the same direction as that of rotation
of the shaft ⑤. The plus and minus signs in Eq. (11) changes at the pitch
point.

In order that gears 1 and 2 can mate at both points M_P and M_Q suc-
cessively, as shown in Fig. 11, the total amount of wear of gears 1 and 2

should be equal at both points M_P and M_Q. The amount of wear w_{P_1} of gear 1 at the point M_P is expressed:

$$w_{P_1} = C_1 f_P P_{nP} U_{sP}/r_{P_1} \tag{12}$$

where C_1 : constant depending upon the gear material

f_P : friction coefficient at M_P

P_{nP} : normal force at M_P

r_{P_1} : radius of curvature of tooth surface at M_P

U_{sP} : sliding velocity at M_P

Supposing that the same material is used for both gears 1 and 2, the total amount of wear of both gears at M_P is expressed as follows:

$$w_P = w_{P_1} + w_{P_2} = C f_P P_{nP} U_{sP}/r_P \tag{13}$$

where $r_P = r_{P_1} r_{P_2}/(r_{P_1} + r_{P_2})$

Considering the average friction coefficient, the following expression is deduced, since w_P is equal to w_Q.

$$(P_n U_s/r)_P = (P_n U_s/r)_Q \tag{14}$$

$$P_{nP} + P_{nQ} = P_n = 2T/D \cos \alpha \tag{15}$$

where D: diameter of pitch circle

Putting $(U_s/r)_P/(U_s/r)_Q = \kappa$, Eqs. (14) and (15) are expressed as follows:

$$P_{nP} = \frac{1}{1+\kappa} P_n, \quad P_{nQ} = \frac{\kappa}{1+\kappa} P_n \tag{16}$$

$$\kappa = \left\{ \frac{(2X-1)}{X(1-X)} \right\}_P \Big/ \left\{ \frac{(2X-1)}{X(1-X)} \right\}_Q$$

The torque due to frictional force F_A on gear-tooth surfaces of (A_1, A_2) gears is expressed:

$$T_{fA} = \phi_{fA} f P_n = \phi_{fA} f (2T/D \cos \alpha) \tag{17}$$

where $\phi_{fA} = \dfrac{-r_{P_2} + \kappa r_{Q_2}}{1+\kappa}$ for mating of two pairs of gear-teeth

$= \mp r_2$ for mating of one pair of gear-teeth

The frictional torque for (B_1, B_2) gears is obtained in the same procedure as for (A_1, A_2) gears. Considering an angle of 2α between both mating lines of (A_1, A_2) and (B_1, B_2), and a discrepancy of $l_n/2$ between the mating positions for (A_1, A_2) and (B_1, B_2), the torque T_f caused by the friction on gear-tooth surfaces is given as sum of T_{fA} and T_{fB} obtained above.

$$T_f = \phi_f f (2T/D \cos \alpha) \tag{18}$$

The frictional torque obtained from the measured value T_M gives a mean value T_{fm} of T_f. Therefore, the following expression is obtained for the average friction coefficient f_m on mating gear-tooth surface in this experiment.

$$f_m = \left(\frac{D \cos \alpha}{2\phi_{fm}}\right)\left(\frac{T_{fm}}{T}\right) \tag{19}$$

The calculation for module $m=4$ yields

$$f_m = 7.56\,T_{fm}/T \tag{20}$$

and Eq. (16) gives the mean normal load as follows:

$$P_{nm} = 0.607 P_n \tag{21}$$

4. 3. Experimental Results

The measurement was carried out in the following range of the average normal load and the rolling velocity:

$$P_{nm} = 30 \text{ to } 130 \text{ kg/cm}, \quad U=1.9 \text{ to } 4.8 \text{ m/s}.$$

The viscosity η of the supplied oil (turbine oil ♯90 and engine oil ♯50) was 0.002 to 0.2 kg·s/m².

Fig. 12 shows the testing results. All data points in the figure are concerned with the combined conditions of four kinds of P_{nm}, four kinds of U and roughly three kinds of η. The results for the disks are shown in a broken line for comparison.

In Fig. 12(a), it appears that the relation between f_m and $\eta U/P_{nm}$ is represented with two lines. The value of f_m is almost constant (about 0.09) for $\eta U/P_{nm}$ below 5×10^{-6}, and it decreases with an increase in $\eta U/P_{nm}$ for $\eta U/P_{nm}$ above 5×10^{-6}. Therefore, the lubrication characteristic on gear-tooth surfaces is classified as follows:

Boundary lubrication $\qquad \eta U/P_{nm} < 5 \times 10^{-6}$

Semi-fluid lubrication $\quad 5 \times 10^{-6} < \eta U/P_{nm} < (5 \times 10^{-4})$

Fluid lubrication $\qquad (5 \times 10^{-4} < \eta U/P_{nm})$

The critical values for $\eta U/P_{nm}$ on the gear-tooth surfaces seem to be ten times greater than those on the disk surfaces. In the region of boundary lubrication, the value of f_m on tooth surfaces is about 1.8 times greater than that on the disk surfaces. In the region of semi-fluid lubrication, the value of f_m is nearly three times greater than that on the disk surfaces for the same value of $\eta U/P_{nm}$, but friction coefficient decreases with an increase in $\eta U/P_{nm}$ in almost same tendency for both gear-tooth surfaces and disk surface.
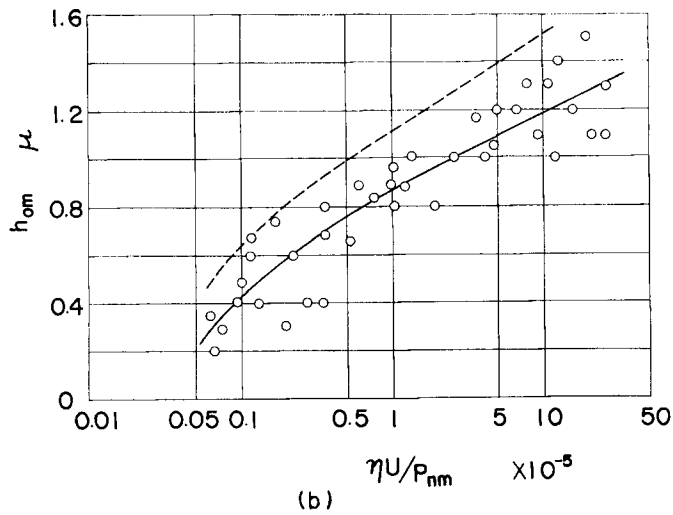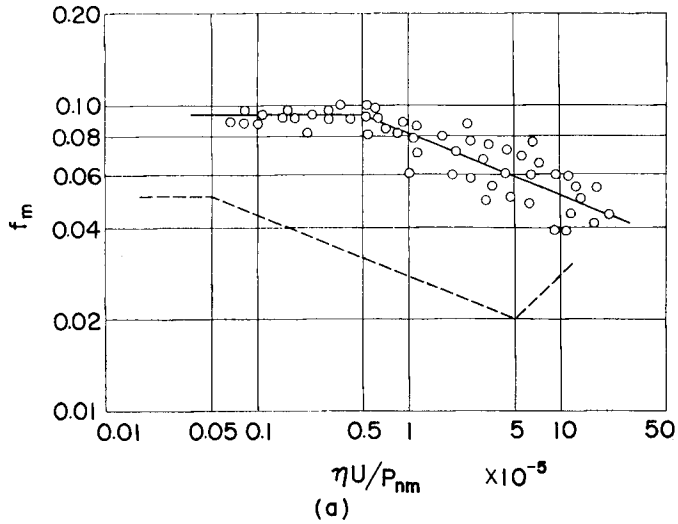
Fig. 12. Friction coefficient and oil-film thickness versus dimensionless
            parameter $\eta U/P_{nm}$.

It is supposed that fluid lubrication in gears may be produced in the range
of $\eta U/P_{nm}$ above 5×10^{-4}. In order to realize fluid lubrication in gears, it is
considered that the rolling velocity is required to be above 25 m/s for an oil
with a comparatively high viscosity of 0.1 kg·s/m² (such as engine oil ♯50 at
17°C) and a comparatively light load of 50 kg/cm. Therefore, it is quite dif-
ficult to realize perfect fluid lubrication in the practical gears.

Fig. 12(b) shows an example of the relation between the average value

of minimum oil-film thickness h_{om} in the gear mating test and $\eta U/P_{nm}$. The broken line is the result obtained when the relative radius of curvature for disks is 10.5 mm (cf. relative radius of curvature for gears used is 7.9 to 10.3 mm).

The average oil-film thickness h_{om} increases with $\eta U/P_{nm}$ for both tests, but the rate of increase is rather small for gears than for disks. Therefore, h_{om} shows much different values in both tests for large values of $\eta U/P_{nm}$. The lubricating effect of oil-film, which is about 1μ thick, upon the gear-tooth surfaces with roughness of 2 to 3μ is quite different from that upon the disk surfaces with roughness of about 1μ, and therefore a great difference is found between the friction coefficient on the mating gear-tooth surfaces and that on the disk surfaces. From these results, it is concluded that the lubrication characteristics are improved in gears as well as in disks with a large value for $\eta U/P_{nm}$.

5. Correlation between Both Lubrication Characteristics on the Disk Surface and the Gear-tooth Surface

If the influence of various factors upon the correlation between both lubrication characteristics on the disk surface and the gear-tooth surface is synthetically clarified, the testing results obtained with rolling disks can be applied to gears more correctly. In the following, the influences of load variation, specific sliding, relative radius of curvature and surface roughness are investigated referring to the previous experimental results.

(1) Influence of load variation on gear-tooth surface

The normal load changes discontinuously with variation of the number of mating gear-teeth, and every gear testing machine has its own dynamic characteristic. The dynamic behaviour was investigated by Buckingham[2], Merritt[3], Niemann[4] and others, and various calculation methods of dynamic load were proposed. These methods show that the value of the load acting on gear-tooth surface used will be 1.4 to 2 times larger than that of the load calculated from the transmitted torque.

(2) Influence of specific sliding

Disks machines are generally driven under the condition of constant specific sliding. The movement of mating point on gear-tooth surface, however, is accompanied by the continuous variation in specific sliding and the change of sliding direction at the pitch point. The value of varying rate of specific sliding on gear-tooth surface is very large. Such a sliding state is quite difficult to realize on disk surfaces.

As shown in Fig. 7(a), specific sliding s has a great effect upon friction coefficient in the range of $s<0.1$, but in the actual gears the value of s is above 0.1 for the most part except in the vicinity of the pitch point. Therefore, specific sliding seems to have little influence upon the average friction coefficient. From Fig. 7(b), it is found that specific sliding has little influence upon oil-film thickness by the same reason as for friction coefficient. However, the influences of the varying rate of specific sliding and the change of sliding direction cannot be clarified.

(3) Influence of relative radius of curvature

The influence of relative radius of curvature r upon friction coefficient can be neglected when the value of r varies in small range. As shown in Fig. 8, oil-film thickness h_0 is proportional to r. The continuous variation of r happens on gear-tooth surfaces, but it is comparatively small.

(4) Influence of roughness of contact surface

As shown in Fig. 9, friction coefficient f varies considerably in the range for small values of H_{max} including 1 to 4μ. The value of f for the ground surface of gear-tooth, H_{max} of which is 2 to 3μ, is 1.3 to 1.6 times greater than that for the super-finished surface. In the region of semi-fluid lubrication, it was observed that oil-film thickness increases with a decrease in H_{max} in the range of H_{max} below 4μ.

In Fig. 13, the broken lines show the transformed results form the ex-

(a)

Fig. 13.

(b)
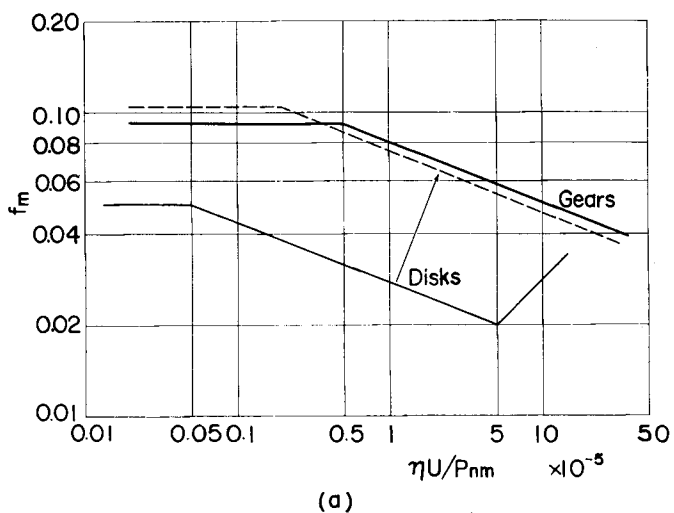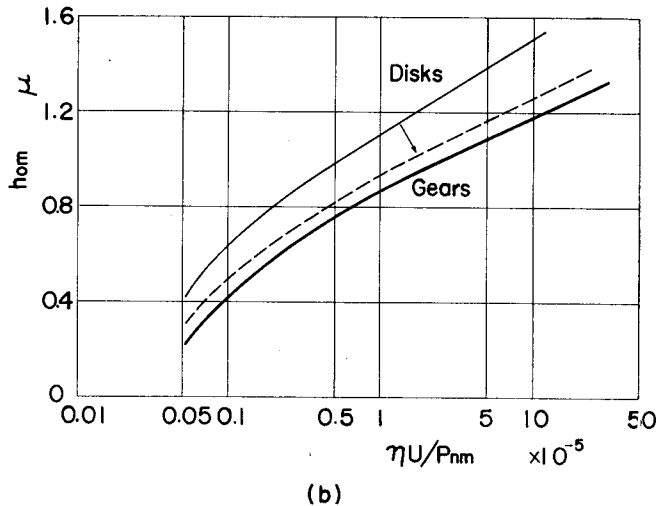
Fig. 13. Correlation between the lubrication characteristics in the disk test and the gear test.

perimental results in the disk machine to gears by taking the above mentioned influences into consideration. In friction coefficient, the transformed result is in a good agreement with the result in the gear test, and in oil-film thickness the transformed result shows a good approach to the result in the gear test. If the influence of other factors is clarified, the transformed results will show a better agreement with the results in the gear test from the average point of view. However, in order to apply the disks to the investigation of the dynamic characteristics of gear lubrication, an adequate device for the dynamic behaviour is required, and the dynamic performance of oil-film is, indeed, one of the most important problems in the field of the fundamental investigation on gear lubrication.

Part II. Fundamental Analysis on Dynamic Phenomena in Gear Lubrication

1. Introduction

Mating of a gear-tooth is intermittent, and oil-film condition between mating gear-tooth surfaces is considered to be quite dynamic. In order to clarify the dynamic performance of oil film, experimental studies were carried out using special models of rollers, and a dynamic lubrication theory was induced. This theory was applied to actual gears taking tooth deflection into consideration, and experimentally the variation of oil-film thickness was measured from the beginning to the ending of a tooth mating. The inves-

tigation, referring to these results, was concerned with the principle of oil-film formation on mating gear-tooth surfaces.

2. Transient Characteristics of Oil-film between Rolling Disks

2. 1. Experimental Equipment and Procedure

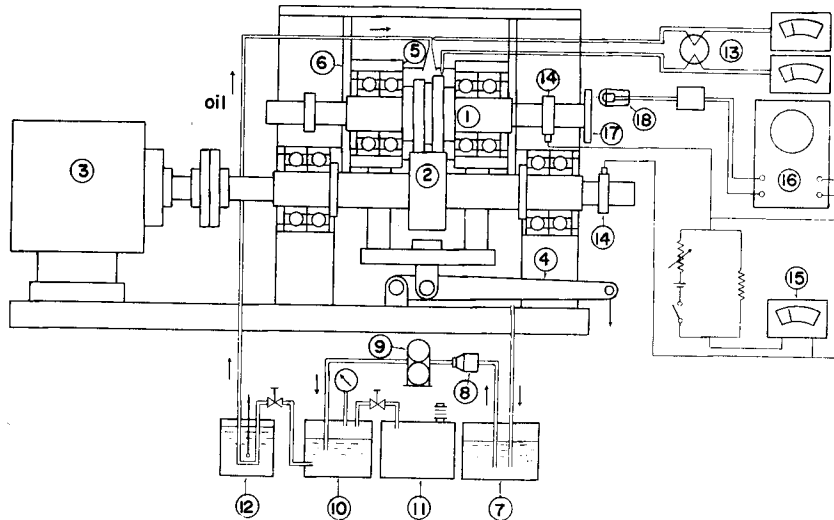The experimental equipment is arranged as shown in Fig. 14.   Testing

Fig. 14.   Arrangement of experimental equipment.

disks ① and ② are manufactured in one body with shaft in order to avoid setting errors.   The variable speed motor ③ drives the testing disk ②, and the special testing disk ① is driven by the friction force on the contact surface with the disk ②.   The bearing housing ⑤ of disk ① can smoothly move up and down along the guides ⑥ which are made of insulating material.   The lubricant supply unit is as shown in the figure.   The variation of oil-film thickness h_0 between two disks is observed by the oscilloscope ⑯ as voltage drop variation.   The rotational position of the disk ① is picked up by the photo-transistor ⑱.   For the disk material, Ni–Cr steel is used.   The contact surface of disk is hardened to $H_R C = 60$ and is ground to $H_{max} < 0.2\mu$.

2. 2. Experimental Results

(1) Effect of discontinuous contact

Mating of a gear-tooth is intermittent and the beginning and the ending of contact happppen discontinuously.   Fig. 15 shows the special testing disk used in this experiment.   It consists of two semi-disks, and oil-film vanishes
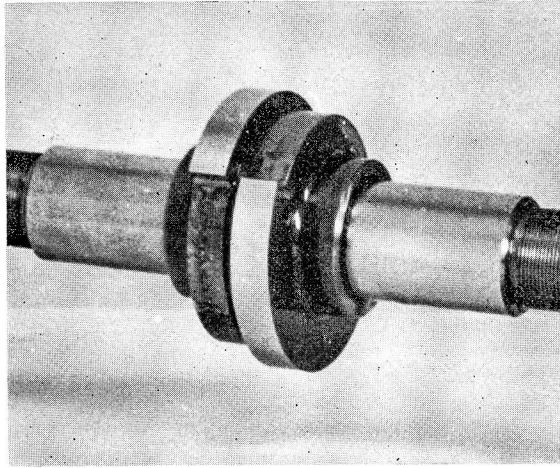
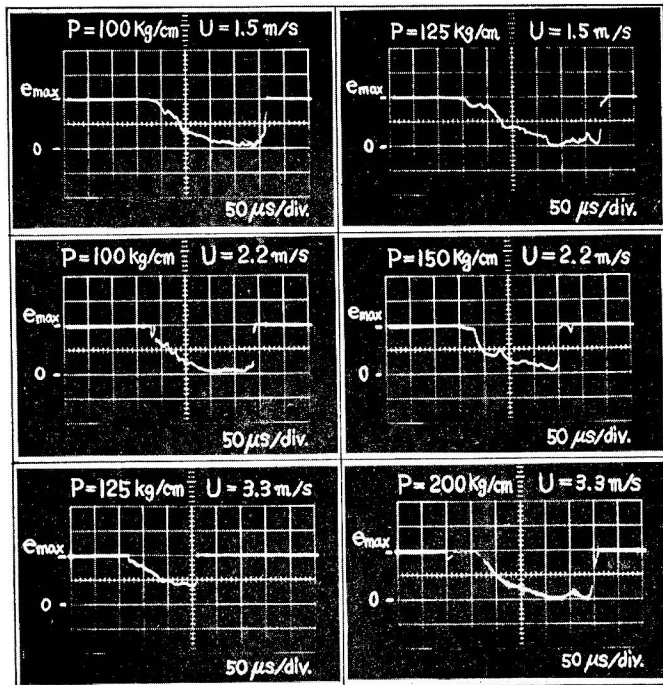Fig. 15. Test disk with discontinuous contact.

Fig. 16. Oscillograms of variation signals of oil-film thickness due to discontinuous contact.

at the edges. Disk diameter is 70 mm, and contact width is 10 mm for each semi-circumference. The testing conditions are as follows:

$$\eta = 0.07 \text{ kg} \cdot \text{s/m}^2, \quad s = 0$$

Fig. 16 shows some oscilloscope traces of h_0 variation signals due to discontinuous contact. Relation between minimum oil-film thickness h_0 and voltage drop e is shown in Fig. 17, and the relation is found to be approximately linear in the region of $h_0 < 0.8\mu$ ($e \leqq 0.085$ V). Maximum voltage drop e_{max} for $h_0 = \infty$ is 0.106 V.

In Fig. 16, every oscillogram shows a steep increase after a gradual decrease of h_0. It is found that the load capacity decreases graduately in the ending part of contact but increases rapidly in the beginning part of contact.
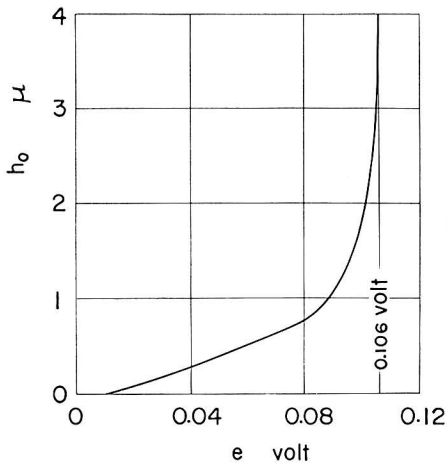

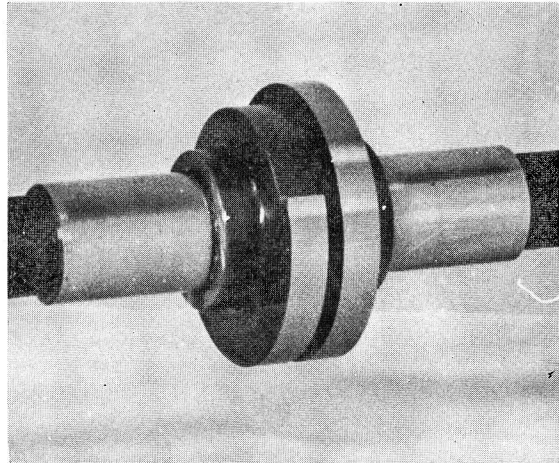Fig. 17. Minimum oil-film thickness versus
voltage drop.

Fig. 18. Test disk with discontinuous change of
contact width

(2) Effect of discontinuous load with contact width change

The force acting on gear-tooth surface changes discontinuously with variation of the number of mating teeth. Fig. 18 shows the testing disk used in this experiment. It consists of an ordinary disk and a semi-disk, and two contact states corresponding to the mating of one pair or two pairs of gear-teeth happens alternately. Disk diameter is 70 mm, and contact width is 10 mm for a semi-circumference and 20 mm for another semi-circumference. The testing conditions are as follows:

$$\eta = 0.05 \text{ kg} \cdot \text{s/m}^2, \quad s = 0$$

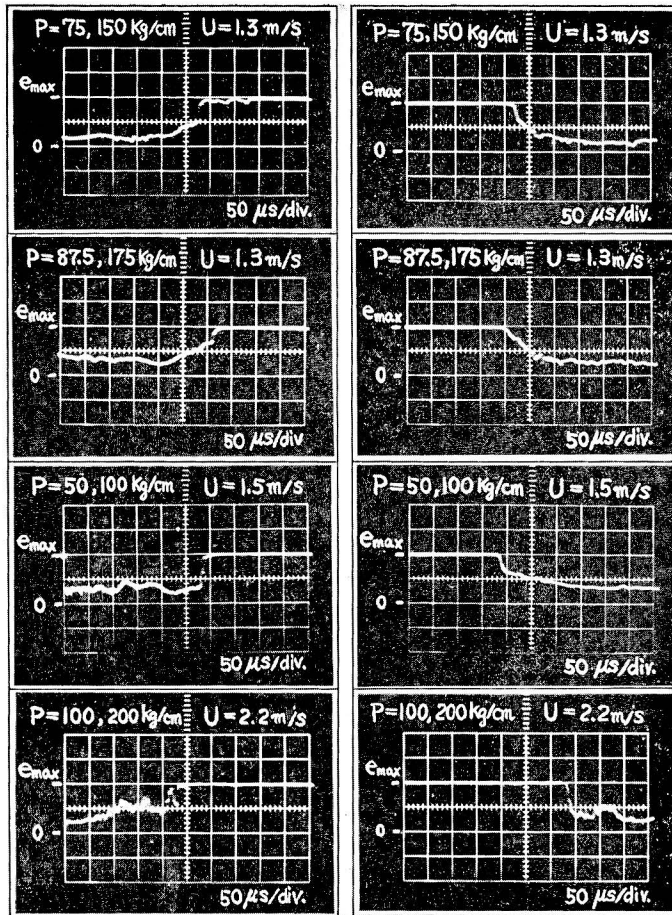Some oscilloscope traces of h_0 variation signals due to discontinuous

Fig. 19. Oscillograms of variation signal of oil-fim thickness due to discontinuous load.

change of contact width are shown in Fig. 19, in which either four results of the left side and the right side show the variation of h_0 with discontinuous increase and decrease of contact width, respectively. It is found that oscillograms show more gradual variation in the states of relatively smaller values of U.

3. Theoretical Analysis on Dynamic Phenomena of oil-film between Rolling Disks

3. 1. General Expressions

By making simle assumptions and neglecting relatively small terms, the equations of motion and continuity reduce to

$$\frac{\partial^2 u}{\partial y^2} = \frac{1}{\eta}\frac{dp}{dx} \tag{22}$$

$$\frac{\partial u}{\partial x}+\frac{\partial v}{\partial y} = 0 \tag{23}$$

where p is pressure in oil-film, and x, y, u, v are the Cartesian coordinates and velocity components (y measures the film thickness).

Eqs. (22) and (23) are applied to a contact of rolling disks shown in Fig. 2. The boundary conditions are as follows:

$$u \doteqdot -U_1 \text{ at } y = -h_1 \quad \text{and} \quad u \doteqdot -U_2 \text{ at } y = h_2$$

$$v = \frac{x}{r_1}U_1 \text{ at } y = -h_1 \quad \text{and} \quad v = \frac{dh_0}{dt}-\frac{x}{r_2}U_2 \equiv V_2-\frac{x}{r_2}U_2 \text{ at } y = h_2$$

where t is time.

In order to perform the integration, following transformations and approximation are made:

$$U = \frac{U_1+U_2}{2}, \quad r \equiv \frac{r_1 r_2}{r_1+r_2}, \quad h = h_1+h_2 \doteqdot h_0\left(1+\frac{x^2}{2rh_0}\right) \tag{24}$$

$$x \equiv \sqrt{2rh_0} \tan\varphi \tag{25}$$

Let V_2 be expressed with a dimensionless parameter λ as follows, because it has a dimension of velocity:

$$V_2 = \frac{dh_0}{dt} \equiv \lambda\sqrt{\frac{2h_0}{r}}\, U \tag{26}$$

Dimensionless factor $\sqrt{2h_0/r}$ is taken into Eq. (26) only for the convenience of calculation. Thus, the pressure distribution becomes

$$p = 3\eta\,\frac{\sqrt{2rh_0}}{h_0^2}\,U\left\{-\lambda Y_1(\varphi)-Y_2(\varphi)+\frac{C_1}{2h_0 U}\,Y_3(\varphi)\right\}+C_2 \tag{27}$$

where $Y_1(\varphi) = 2\cos^4\varphi, \quad Y_2(\varphi) = 2(\varphi+\sin\varphi\cos\varphi)$

$Y_3(\varphi) = 3\varphi+3\sin\varphi\cos\varphi+2\sin\varphi\cos^3\varphi$

Integral constants in Eq. (27) are obtained from the following boundary conditions:

$$p = 0 \text{ at } x = x_1, (\varphi = \varphi_1) \quad \text{and} \quad x = x_2, (\varphi = \varphi_2) \qquad (x_2 \geqq x_1)$$

Eq. (27) becomes

$$p = 3\eta\,\frac{\sqrt{2rh_0}}{h_0^2}\,U\{\lambda I_1(\varphi)+I_2(\varphi)\} \equiv \eta\,\frac{\sqrt{2rh_0}}{h_0^2}\,U\Psi(\varphi) \tag{28}$$

where $I_j(\varphi) = -Y_j(\varphi)+\dfrac{[Y_j(\varphi_1)-Y_j(\varphi_2)]Y_3(\varphi)-[Y_j(\varphi_1)Y_3(\varphi_2)-Y_j(\varphi_2)Y_3(\varphi_1)]}{Y_3(\varphi_1)-Y_3(\varphi_2)}$

$$(j=1, 2)$$

The load capacity per unit width P is obtained by integrating Eq. (28)

over the interval x_1 to x_2.

$$P = \eta \frac{Ur}{h_0} K(\varphi_1, \varphi_2) = P_d + P_c, \quad K = \lambda K_d + K_c \tag{29}$$

where

$$K_d = -6\Big[(\varphi + \sin\varphi\cos\varphi)$$
$$+ \frac{[Y_1(\varphi_1)\{3\varphi - Y_3(\varphi_2)\} - Y_1(\varphi_2)\{3\varphi - Y_3(\varphi_1)\}]\tan\varphi - [Y_1(\varphi_1) - Y_1(\varphi_2)]\cos^2\varphi}{Y_3(\varphi_2) - Y_3(\varphi_1)}\Big]_{\varphi_1}^{\varphi_2}$$

$$K_c = 6\Big[\frac{[Y_3(\varphi_1)\{2\varphi - Y_2(\varphi_2)\} + \varphi\{3Y_2(\varphi_2) - 2Y_3(\varphi_2)\} - Y_2(\varphi_1)\{3\varphi - Y_3(\varphi_2)\}]\tan\varphi}{Y_3(\varphi_2) - Y_3(\varphi_1)}$$
$$+ [Y_2(\varphi_1) - Y_2(\varphi_2)]\cos^2\varphi\Big]_{\varphi_1}^{\varphi_2}$$

Particularly, if

$$\frac{dp}{dx} = 0 \quad \text{at} \quad x_1 = x_A \quad \text{or} \quad \varphi_1 = \varphi_A,$$

λ is obtained as follows:

$$\lambda\Big\{\tan\varphi_A + \frac{Y_1(\varphi_A) - Y_1(\varphi_2)}{Y_3(\varphi_A) - Y_3(\varphi_2)}\Big\} = \Big\{0.5\sec^2\varphi_A - \frac{Y_2(\varphi_A) - Y_2(\varphi_2)}{Y_3(\varphi_A) - Y_3(\varphi_2)}\Big\} \tag{30}$$

The value of φ_A depends upon the state of oil-film, and it is obtained from the condition that the load capacity has the same value as the load.

If $\varphi_2 = \pi/2$ and $\varphi_1 = \varphi_A$ ($\equiv\varphi_{A\alpha}$), Eqs. (29) and (30) become

$$\left.\begin{aligned}
K &\equiv K_\alpha = \lambda K_{d\alpha} + K_{c\alpha}\\
K_{d\alpha} &= \frac{-6}{1.5\pi - Y_3(\varphi_{A\alpha})}[\{0.5\pi - (\varphi_{A\alpha} + \sin\varphi_{A\alpha}\cos\varphi_{A\alpha})\}\{1.5\pi - Y_3(\varphi_{A\alpha})\}\\
&\qquad + Y_1(\varphi_{A\alpha})\cos^2\varphi_{A\alpha} - 3Y_1(\varphi_{A\alpha})\{1 + (\varphi_{A\alpha} - 0.5\pi)\tan\varphi_{A\alpha}\}]\\
K_{c\alpha} &= \frac{-6}{1.5\pi - Y_3(\varphi_{A\alpha})}[\{2Y_3(\varphi_{A\alpha}) - 3Y_2(\varphi_{A\alpha})\}\{1 + (\varphi_{A\alpha} - 0.5\pi)\tan\varphi_{A\alpha}\}\\
&\qquad + \{Y_2(\varphi_{A\alpha}) - \pi\}\cos^2\varphi_{A\alpha}]
\end{aligned}\right\} \tag{31}$$

$$\lambda = \frac{0.5\sec^2\varphi_{A\alpha}[Y_3(\varphi_{A\alpha}) - 1.5\pi] - [Y_2(\varphi_{A\alpha}) - \pi]}{\tan\varphi_{A\alpha}[Y_3(\varphi_{A\alpha}) - 1.5\pi] + Y_1(\varphi_{A\alpha})} \tag{32}$$

3.2. Numerical analysis

(1) Effect of discontinuous contact

From Fig. 20, which shows the contact state of the test disks mentioned previously, the boundary conditions of pressure distribution become as follows:

$p = 0$ at $\varphi_1 = \varphi_t$ and $\varphi_2 = \pi/2$ for the biginning part of contact (β) (33)

$p = 0$ at $\varphi_1 = \varphi_{A\gamma}$ and $\varphi_2 = \varphi_t$, and $dp/dx = 0$ at $\varphi_1 = \varphi_{A\gamma}$

for the ending part of contact (γ) (34)

By substituting these condition into Eqs. (29) and (30), following expressions
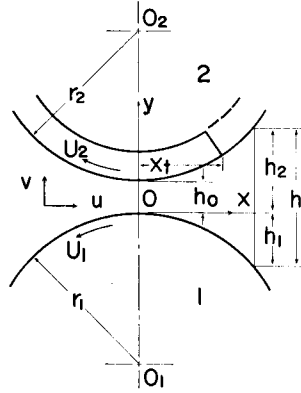
Fig. 20. Contact of rolling disks
with discontinuous contact
between which oil-film is
formed.

are obtained :

$$K_{d\beta} = \frac{-6}{1.5\pi - Y_3(\varphi_t)} [\{0.5\pi - (\varphi_t + \sin\varphi_t \cos\varphi_t)\}\{1.5\pi - Y_3(\varphi_t)\}$$
$$+ Y_1(\varphi_t)\cos^2\varphi_t - 3Y_1(\varphi_t)\{1 + (\varphi_t - 0.5\pi)\tan\varphi_t\}]$$

$$K_{c\beta} = \frac{-6}{1.5\pi - Y_3(\varphi_t)} [\{2Y_3(\varphi_t) - 3Y_2(\varphi_t)\}\{1 + (\varphi_t - 0.5\pi)\tan\varphi_t\}$$
$$+ \{Y_2(\varphi_t) - \pi\}\cos^2\varphi_t]$$

$$\left. \right\} \quad (35)$$

$$K_{d\gamma} = \frac{-6}{Y_3(\varphi_t) - Y_3(\varphi_{A\gamma})} [(\varphi + \sin\varphi\cos\varphi)\{Y_3(\varphi_t) - Y_3(\varphi_{A\gamma})\} - \{Y_1(\varphi_{A\gamma})$$
$$- Y_1(\varphi_t)\}\cos^2\varphi + (Y_1(\varphi_{A\gamma})\{3\varphi - Y_3(\varphi_t)\}$$
$$- Y_1(\varphi_t)\{3\varphi - Y_3(\varphi_{A\gamma})\})\tan\varphi]_{\varphi_{A\gamma}}^{\varphi_t}$$

$$K_{c\gamma} = \frac{6}{Y_3(\varphi_t) - Y_3(\varphi_{A\gamma})} [(Y_3(\varphi_{A\gamma})\{2\varphi - Y_2(\varphi_t)\} + \varphi\{3Y_2(\varphi_t) - 2Y_3(\varphi_t)\}$$
$$- Y_2(\varphi_{A\gamma})\{3\varphi - Y_3(\varphi_t)\})\tan\varphi$$
$$+ \{Y_2(\varphi_{A\gamma}) - Y_2(\varphi_t)\}\cos^2\varphi]_{\varphi_{A\gamma}}^{\varphi_t}$$

$$\left. \right\} \quad (36)$$

$$\lambda\left\{\tan\varphi_{A\gamma} + \frac{Y_1(\varphi_{A\gamma}) - Y_1(\varphi_t)}{Y_3(\varphi_{A\gamma}) - Y_3(\varphi_t)}\right\} = \left\{0.5\sec^2\varphi_{A\gamma} - \frac{Y_2(\varphi_{A\gamma}) - Y_2(\varphi_t)}{Y_3(\varphi_{A\gamma}) - Y_3(\varphi_t)}\right\} \quad (37)$$

Now, the steady state in the ordinary disks contact is taken as the standard state, and the state is expressed with a subscript b. By putting λ into zero in Eq. (32), -0.4436 is obtained as the value of $\varphi_{A\alpha b}$, and Eq. (29) becomes

$$P_b = \eta\frac{Ur}{h_{0b}}K_b \qquad \text{where} \quad K_b = 4.896 \qquad (38)$$

The inertia force due to vertical motion of the disk is calculated. The velocity at which two disks approach is expressed as Eq. (26). Therefore, the acceleration a becomes

$$a = \frac{dV_2}{dt} = \frac{d\lambda}{dt}\sqrt{\frac{2h_0}{r}}\,U + \frac{(\lambda U)^2}{r} \tag{39}$$

Let's consider a dimensionless parameter Θ referring to time t as follows:

$$\Theta = \frac{U}{\sqrt{2rh_0}}\,t \tag{40}$$

Then, a becomes

$$a = \frac{U^2}{r}\left(\frac{d\lambda}{d\Theta} + \lambda^2\right) \tag{41}$$

The inertia force W_t becomes

$$W_t = \left(\frac{W_D}{g}\right)a = W_D\,\frac{U^2}{gr}\left(\frac{d\lambda}{d\Theta} + \lambda^2\right) \tag{42}$$

where W_D: disk weight, g: acceleration of gravity.

The actual load W_E is expressed as the sum of the imposed load W and the inertia force W_t.

$$W_E = W + W_t = W\left\{1 + \frac{W_D}{W}\frac{U^2}{gr}\left(\frac{d\lambda}{d\Theta} + \lambda^2\right)\right\} \equiv W\left\{1 + \zeta\left(\frac{d\lambda}{d\Theta} + \lambda^2\right)\right\} \tag{43}$$

The imposed load W is equal to the standard value W_b. Because the actual load is supported by the both parts of β and γ, the following relation is obtained:

$$\frac{K_\beta + K_\gamma}{h_0} = \frac{K_b}{h_{0b}}\left\{1 + \frac{W_D}{W_b}\frac{U^2}{gr}\left(\frac{d\lambda}{d\Theta} + \lambda^2\right)\right\} = \frac{K_b}{h_{0b}}\left\{1 + \zeta_b\left(\frac{d\lambda}{d\Theta} + \lambda^2\right)\right\} \tag{44}$$

The oil-film thickness in transient state is calculated as follows. From Eq. (25), the x-coordinate of the discontinuous contact edge becomes

$$x_t = \sqrt{2rh_0}\,\tan\varphi_t$$

By differentiating this equation and substituting Eq. (26) into it supposing λ is constant during a short period dt,

$$\frac{dh_0}{h_0} = -\frac{2\lambda U}{U_2}\frac{\sec^2\varphi_t}{(\lambda U/U_2)\tan\varphi_t + 1}\,d\varphi_t$$

The initial condition is as follows:

$$h_0 = h_{0a} \quad \text{at} \quad \varphi_t = \varphi_a$$

By integrating the above differential equation, h_0 at $\varphi_t = \varphi_a + d\varphi_t$ is obtained as follows:

$$h_0 = h_{0a}\left\{\left(\lambda\frac{U}{U_2}\tan\varphi_A + 1\right)\middle/\left(\lambda\frac{U}{U_2}\tan\varphi_t + 1\right)\right\}^2 \tag{45}$$

From Eqs. (26) and (45), the increment $dt(=t-t_a)$ corresponding to $d\varphi_t(=\varphi_t-\varphi_a)$

becomes

$$t - t_a = \frac{\sqrt{r}}{\sqrt{2}\,\lambda U}\left(\frac{h_0}{\sqrt{h_{0a}}} - \sqrt{h_{0a}}\right) \tag{46}$$

Therefore,

$$\Theta - \Theta_a = \frac{1}{2\lambda}\left(1 + \sqrt{\frac{h_0}{h_{0a}}}\right)\left(\sqrt{\frac{h_0}{h_{0b}}} - \sqrt{\frac{h_{0a}}{h_{0b}}}\right) \tag{47}$$

According to the above relations, variation of oil-film thickness due to discontinuous contact is numerically calculated. The results are shown in Fig. 21. From Eq. (44), for example, $\zeta_b = 1$ corresponds to a following case.
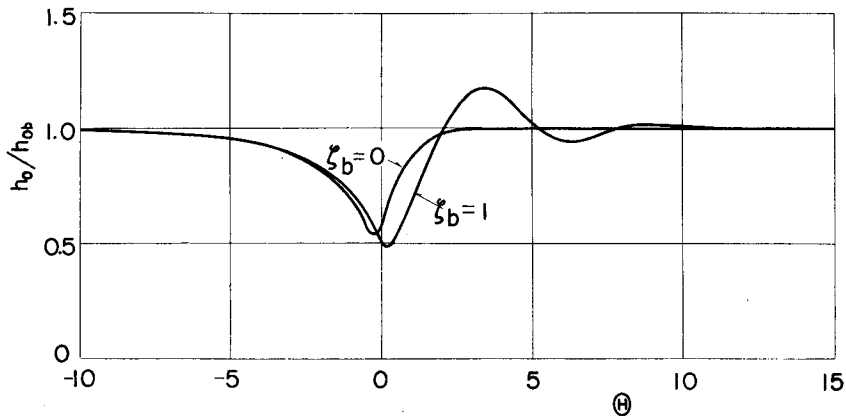

Fig. 21. Variation of oil-film thickness due to discontinuous contact.

$W_D = 1.5\,\mathrm{kg}$, $r = 17.5\,\mathrm{mm}$ (values for test disk before-mentioned)
$W_b = 150\,\mathrm{kg}$, $U = 4.16\,\mathrm{m/s}$

Horizontal scale Θ is taken as follows, according to Eqs. (40) and (47):

$$\Theta = 0 \quad \text{at} \quad x_t = 0 \quad \text{and} \quad \Theta < 0 \quad \text{at} \quad x_t > 0$$

In the figure, h_0 takes minimum value in the neighbourhood of $\Theta = 0$. The minimum value for $\zeta_b = 1$ is rather smaller than that for $\zeta_b = 0$, and h_0 for $\zeta_b = 1$ shows oscillatory variation and is behind h_0 for $\zeta_b = 0$ in progress of variation. These characteristics are due to the influence of inertia force. In general, the variation of h_0 shows a steep increase after a gradual decrease, and this characteristic is in good agreement with the experimental results shown in Fig. 16. The transient state of oil-film seems to continue for $t > 0.35\,\mathrm{ms}$ in Fig. 16 and $\Theta = 12$ to 20 in Fig. 21. From the testing conditions, it is calculated that $\Theta = 12$ to 20 corresponds to $t = 1.2$ to 2 ms. One of the causes of this difference is thought to be that the variation of voltage drop is very small in the range of $h_0 > 2\mu$, as shown in Fig. 17.

(2) Effect of discontinuous load with contact width change

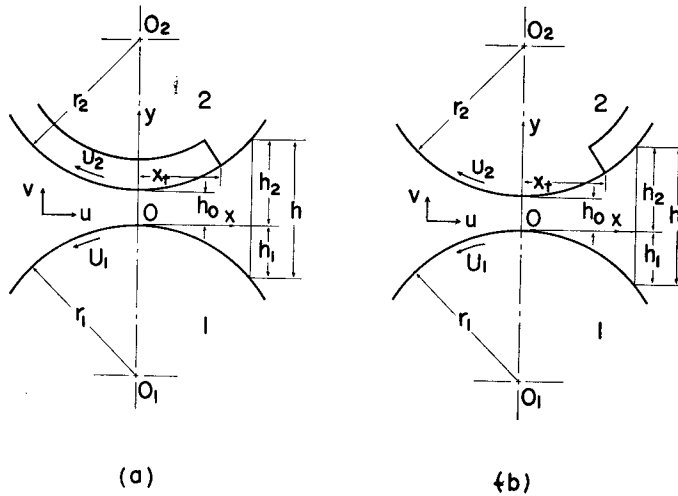Fig. 22 shows the contact state of model disks whose contact width

Fig. 22. Contact of rolling disks with discontinuous change of contact width between which oil-film is formed.

change discontinuously. For the ordinary disk part a, the expressins of K and λ become Eqs. (31) and (32). The boundary conditions of pressure distribution for the beginning part of contact (β) become Eq. (33), and for the ending part of contact (γ) Eq. (34). Therefore, the expressions of K and λ for these parts become Eqs. (35), (36) and (37).

Because the load is supported by the both parts a and β or a and γ, the following relations are obtained.

$$\frac{K_a + K_\beta}{h_0} = \frac{K_b}{h_{ob}}\left\{1 + \zeta_b\left(\frac{d\lambda}{d\Theta} + \lambda^2\right)\right\} \quad \text{for the increase of contact width} \quad (48)$$

$$\frac{K_a + K_\gamma}{h_0} = \frac{K_b}{h_{ob}}\left\{1 + \zeta_b\left(\frac{d\lambda}{d\Theta} + \lambda^2\right)\right\} \quad \text{for the decrease of contact width} \quad (49)$$

The oil-film thickness in transient state is calculated by Eqs. (45) and (47).

Fig. 23 shows the numerical results. In the figure, (a) and (b) show the variation of h_0 with an increase and a decrease of contact width, respectively. The variation of h_0 with a decrease of contact width shows a more early progress than that with an increase of contact width. The transient states of oil-film seems to continue for $\Theta = 10$ to 20, which corresponds to $t = 1$ to 2 ms. In the experimental results shown in Fig. 19, the length of this time is less than 0.3 ms. The cause of this difference was previously mentioned.

From these results, it is found that the transient state of oil-film can be
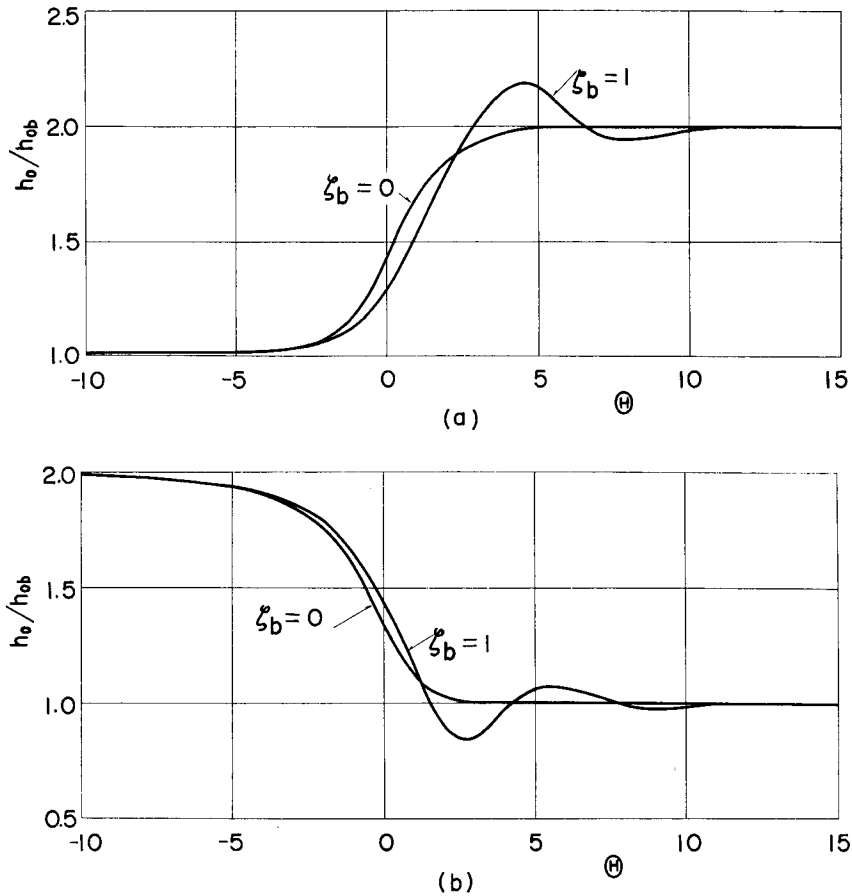
Fig. 23.   Variation of oil-film thickness due to discontinuous load.

fundamentally expressed by the dynamic lubrication theory.

4.   Theoretical Analysis on Dynamic Phenomena of Oil-film between Mating Gear-tooth Surfaces

4. 1.   Analysis on Dynamic Phenomena of Lubricated Gear-tooth under Loading

Fig. 24 shows a relative position of two pairs of gear-teeth I and II, which are mating at the same time, on the basis of the position of the pair I.

The relations between W and δ are as follows :

$$W_I = k_I \delta_I , \quad W_{II} = k_{II} \delta_{II} \tag{50}$$

Because two pairs I and II can be mating at the same time only when the resultant error of normal pitch of the pair I is equal to that of the pair II,
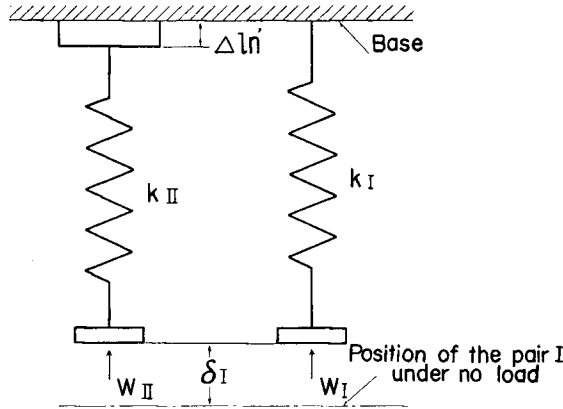
k : stiffness of a pair of
    mating teeth
W : normal load on tooth surface
δ : variation of normal pitch
    due to tooth deflection
$\Delta l_n'$: resultant manufacturing
    error of normal pitch for
    two gears

Fig. 24. Relative position of two pairs of gear-teeth mating
at the same time.

$$\delta_{II} = \delta_I + \Delta l_n' \tag{51}$$

Let's suppose that the mating of the pair I happens previous to that of the pair II. At the beginning of mating of the pair II, the effective normal pitch l_{nE} becomes as follows, because δ_{II} is zero:

$$l_{nE} = l_n - (\delta_I + \Delta l_n') \tag{52}$$

where l_n : regular normal pitch

By H. Walker[5], δ becomes larger than 10μ even under relatively light load, but $\Delta l_n'$ is not over 10μ in the precision gears, whose tooth surface is finished by grinding. Therefore, in general, $(\delta_I + \Delta l_n')$ is positive, and l_{nE} is smaller than l_n.

Fig. 25 shows schematically the mating states of two pairs of gear-teeth. In the figure, $\Delta l_n'$ is neglected but the figure holds the generality because $(\delta_I + \Delta l_n')$ is positive.

From Fig. 25, the resultant errors of normal pitch Δl_{nI} and Δl_{nII}, due to the deflection δ_I and δ_{II} and oil-film thickness h_{0I} and h_{0II}, becomes as follows:

$$\Delta l_{nI} = -\delta_I + h_{0I}, \quad \Delta l_{nII} = -\delta_{II} + h_{0II} \tag{53}$$

1, 2 : two pieces of mating gears
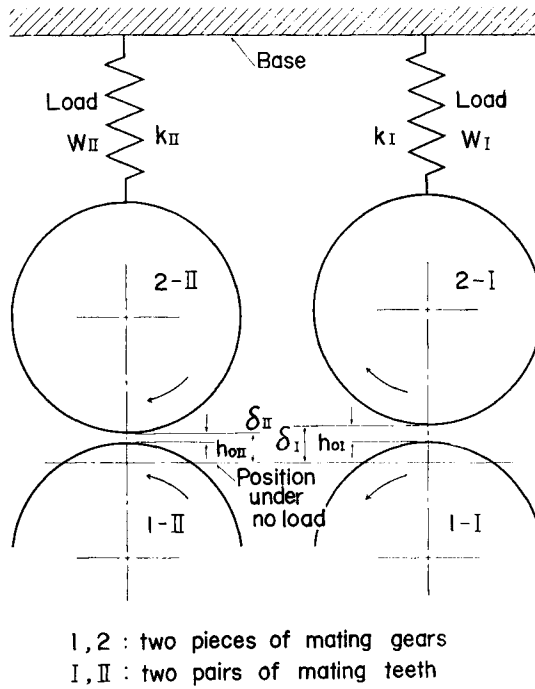I, II : two pairs of mating teeth

Fig. 25. Contact of two pairs of rolling disks, corresponding
to two pairs of mating gear-teeth.

When two pairs I and II are mating at the same time,

$$\varDelta l_{nI} = \varDelta l_{nII}$$

Therefore, following expression is obtained:

$$h_{0II} = h_{0I} - (\delta_I - \delta_{II}) \tag{54}$$

At the beginning of mating of the pair II, δ_{II} is zero.

$$h_{0II} = h_{0I} - \delta_I \tag{55}$$

Because the thickness of oil-film, formed between mating tooth surfaces, is several microns at the most, h_{0II} is generally negative at the beginning of mating. But this result does'nt always mean the interference, as shown in Fig. 26. From the figure, it is found that h_{0II} is an imaginary minimum thickness and the actual minimum thickness is h_{0t}.

After all, in order to clarify the principle of oil-film formation in gears, the case of $h_0 < 0$ has to be analyzed as well as the case of $h_0 > 0$.

4. 2. General Expressions

This section refers only to the case of $h_0 < 0$, because the case of $h_0 > 0$
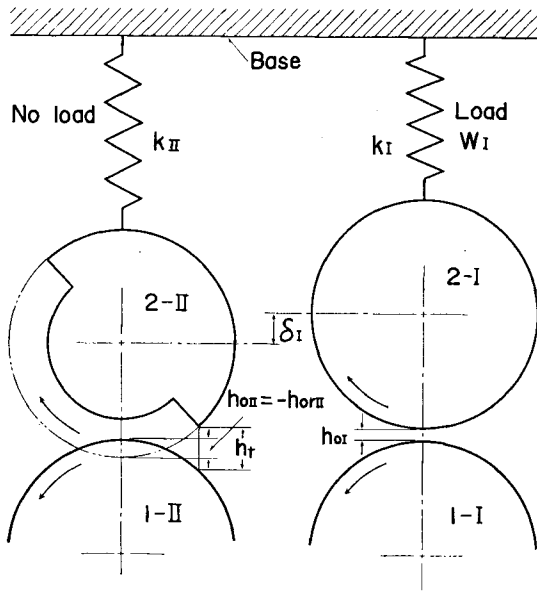
Fig. 26. Contact of two pairs of rolling disks, corresponding to the beginning of mating of a pair of teeth.
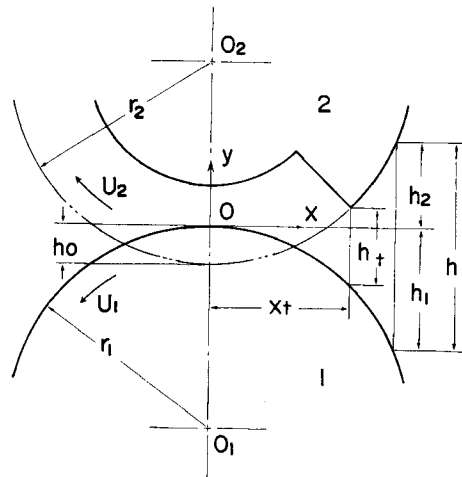
Fig. 27. Contact of rolling disks, corresponding to the beginning state of mating.

was previously analyzed. Fig. 27 shows the contact of rolling disks in the case of $h_0 < 0$. Now, following transformations are made.

$$h_0 \equiv -h_{0r} < 0 \tag{56}$$

$$x \equiv \sqrt{2rh_{0r}}\ \sec\psi \tag{57}$$

$$V_2 \equiv \lambda\sqrt{\frac{2h_{0r}}{r}}\ U \tag{58}$$

The boundary conditions of pressure distribution are as follows:

$$p = 0 \quad \text{at} \quad x = x_1,\ (\psi = \psi_1) \quad \text{and} \quad x = x_2,\ (\psi = \psi_2) \qquad (x_2 \geqq x_1)$$

Thus, from Eqs. (22) and (23), the pressure distribution is obtained as follows:

$$p = 3\eta\,\frac{\sqrt{2rh_{0r}}}{h_{0r}^2}\,U\{\lambda I_1'(\psi) + I_2'(\psi)\} \equiv \eta\,\frac{\sqrt{2rh_{0r}}}{h_{0r}^2}\,U\Psi'(\psi) \tag{59}$$

where $\quad I_j'(\psi) = -Y_j'(\psi) + \dfrac{\{Y_j'(\psi_1) - Y_j'(\psi_2)\}\,Y_3'(\psi) - \{Y_j'(\psi_1)Y_3'(\psi_2) - Y_j'(\psi_2)Y_3'(\psi_1)\}}{Y_3'(\psi_1) - Y_3'(\psi_2)}$

$\quad (j = 1, 2)$

$\quad Y_1'(\psi) = 2\cot^4\psi, \quad Y_2'(\psi) = -2\{\cot\psi\,\mathrm{cosec}\,\psi + \log|\tan(\psi/2)|\}$

$\quad Y_3'(\psi) = \cot\psi\,\mathrm{cosec}\,\psi(3 - 2\cot^2\psi) + 3\log|\tan(\psi/2)|$

The load capacity per unit width P is obtained by integrating Eq. (59) over the interval x_1 to x_2.

$$P = \eta \frac{Ur}{h_{0r}} K'(\psi_1, \psi_2) = P_d + P_c, \quad K' = \lambda K'_d + K'_c \tag{60}$$

where

$$K'_d = \frac{-6}{Y'_3(\psi_2) - Y'_3(\psi_1)} \Bigg[\Big((\cot \psi \operatorname{cosec} \psi + \log \Big| \tan \frac{\psi}{2} \Big|) \{ Y'_3(\psi_1) - Y'_3(\psi_2) \}$$

$$+ \Big(\cot^2 \psi + 3 \sec \psi \log \Big| \tan \frac{\psi}{2} \Big| \Big) \{ Y'_1(\psi_1) - Y'_1(\psi_2) \}$$

$$- \{ Y'_1(\psi_1) Y'_3(\psi_2) - Y'_1(\psi_2) Y'_3(\psi_1) \} \sec \psi \Bigg]_{\psi_1}^{\psi_2}$$

$$K'_c = \frac{6}{Y'_3(\psi_2) - Y'_3(\psi_1)} \Bigg[-2 \sec \psi \log \Big| \tan \frac{\psi}{2} \Big| \{ Y'_3(\psi_1) - Y'_3(\psi_2) \}$$

$$- \Big(\cot^2 \psi + 3 \sec \psi \log \Big| \tan \frac{\psi}{2} \Big| \Big) \{ Y'_2(\psi_1) - Y'_2(\psi_2) \}$$

$$+ \{ Y'_2(\psi_1) Y'_3(\psi_2) - Y'_2(\psi_2) Y'_3(\psi_1) \} \sec \psi \Bigg]_{\psi_1}^{\psi_2}$$

In the case of $h_0 < 0$, following condition must be satisfied:

$$x_2 \geqq x_1 > 0 \qquad \text{for the beginning of mating}$$
$$0 > x_2 \geqq x_1 \qquad \text{for the ending of mating}$$

The latter is negligible except the squeeze action has a large effect upon the load capacity, because the pressure due to the wedge effect grows mostly in the positive part of x.

4.3. Numerical Analysis

In the case of $h_0 > 0$, the states of oil-film are expressed by following equations:

For the perfect mating: Eqs. (31) and (32)

For the beginning of mating: Eq. (35)

For the ending of mating: Eqs. (36) and (37)

In the case of $h_0 < 0$, the boundary conditions of pressure distribution for the beginning of mating are as follows:

$$p = 0 \quad \text{at} \quad \psi_1 = \psi_t \quad \text{and} \quad \psi_2 = \pi/2$$

By substituting these conditions into Eq. (60), the load capacity is obtained as follows:

$$\left. \begin{aligned} K'_{d\beta} &= \frac{-6}{Y'_3(\psi_t)} \Big\{ Y'_3(\psi_t) \Big(\cot \psi_t \operatorname{cosec} \psi_t + \log \Big| \tan \frac{\psi_t}{2} \Big| \Big) \\ &\quad + Y'_1(\psi_t) \Big(\cot^2 \psi_t + 3 \sec \psi_t \log \Big| \tan \frac{\psi_t}{2} \Big| + 3 \Big) \Big\} \\ K'_{c\beta} &= \frac{-6}{Y'_3(\psi_t)} \Big\{ 2 Y'_3(\psi_t) \Big(1 + \sec \psi_t \log \Big| \tan \frac{\psi_t}{2} \Big| \Big) \\ &\quad + Y'_2(\psi_t) \Big(\cot^2 \psi_t + 3 \sec \psi_t \log \Big| \tan \frac{\psi_t}{2} \Big| + 3 \Big) \end{aligned} \right\} \tag{61}$$

From Eqs. (35) and (61), a following relation is obtained.

$$\lim_{h_0 \to 0} K(\varphi_t, \pi/2) = \lim_{h_0r \to 0} K'(\psi_t, \pi/2)$$

When a pair of gears is driven under a contact load, the load capacities of oil-film between mating teeth satisfy the following relation, if the dynamic load is negligible.

$$\left(\frac{\eta U r}{h_0} K\right)_{\mathrm{I}} + \left(\frac{\eta U r}{|h_0|} K\right)_{\mathrm{II}} = \left(\frac{\eta U r}{h_0} K\right)_b \tag{62}$$

where I: α, II: β or γ

When only one pair of teeth is mating, $K_{\mathrm{II}}=0$. In the case of $h_{0\mathrm{II}}=h_{0\beta}<0$, K_{II} and $h_{0\mathrm{II}}$ become K'_{β} and $h_{0r\beta}$, respectively. The steady state under the driving condition of one pair of teeth mating is taken as the standard state, which corresponds to the right side of Eq. (62). When the dynamic load is taken into consideration, the right side of Eq. (62) varies. When two pairs of gear-teeth are mating at the same time, the relation as shown in Eq. (54) has to be satisfied. In Eq. (50), supposing that δ is the deflection due to the load per unit width P,

$$\delta = \frac{P}{k} = \frac{\eta U r}{k} \frac{K}{|h_0|} \tag{63}$$

Because $(\eta U r/k)$ has a dimension of square of length, following expression is capable:

$$\delta = q h_{0b}{}^2 \frac{K}{|h_0|} \tag{64}$$

where q: dimensionless parameter

By substituting Eq. (64), Eq. (54) becomes as follows:

$$-q_{\mathrm{I}} h_{0b}{}^2 \frac{K_{\mathrm{I}}}{h_{0\mathrm{I}}} + h_{0\mathrm{I}} = -q_{\mathrm{II}} h_{0b}{}^2 \frac{K_{\mathrm{II}}}{|h_{0\mathrm{II}}|} + h_{0\mathrm{II}} \tag{65}$$

In the case of $h_0 > 0$, the oil-film thickness in transient state is calculated according to Eqs. (45), (46) and (47). In the case of $h_0 < 0$, following expressions are obtained in the same procedure as in the case of $h_0 > 0$:

$$h_{0r} = h_{0ra} \left\{\left(\lambda \frac{U}{U_2} \sec \psi_a - 1\right) \Big/ \left(\lambda \frac{U}{U_2} \sec \psi_t - 1\right)\right\}^2 \tag{66}$$

$$\Theta - \Theta_a = \frac{1}{2\lambda}\left(1 + \sqrt{\frac{h_0}{h_{0ra}}}\right)\left(\sqrt{\frac{h_{0r}}{h_{0b}}} - \sqrt{\frac{h_{0ra}}{h_{0b}}}\right) \tag{67}$$

By expressing various factors as functions of time t and substituting them into the above equations, the transient state of oil-film between mating gear-tooth surfaces is obtained. Fig. 28 shows variation of oil-film thickness
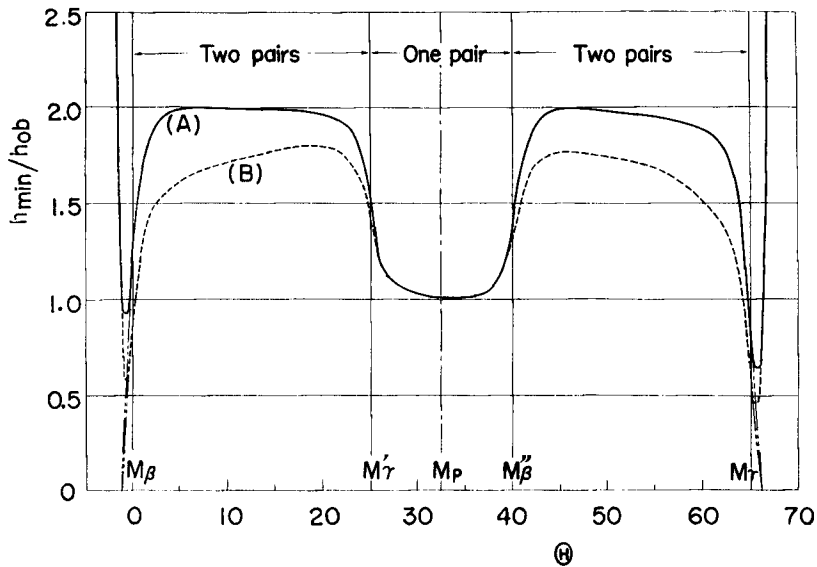
$M\beta$, $(M\overset{''}{\beta})$: beginning point of regular mating (succeeding tooth)

$M\gamma$, $(M\overset{'}{\gamma})$: ending point of regular mating (preceding tooth)

M_p : pitch point

Fig. 28. Variation of oil-film thickness on the mating gear-tooth surface.

which is numerically calculated.

In the figure, Θ shows the value obtained by supposing $h_{ob}=1\mu$ in the case of the test gears used in the following experiment. The main dimensions are shown in Table 1. Two curves shown in the figure are obtained by the following assumptions:

(A) Viscosity, rolling velocity, relative radius of curvature, and resultant tooth stiffness are constant in all the range of mating. Calculation is performed at $q=0.5$. From Eqs. (63) and (64), for example, this corresponds to a following case:

$$\eta = 0.01 \, \text{kg·s/m}^2, \quad U = 10 \, \text{m/s}, \quad r = 10 \, \text{mm},$$
$$k = 2\times10^4 \, (\text{kg/cm})/\text{mm}, \quad h_{ob} = 1\mu.$$

There is no acting of the dynamic load, and the total load is constant.

(B) The variation of relative radius of curvature is taken into consideration, and q varies from 0.335 (at the beginning and the ending of mating) to 0.5 (at the pitch point). Other assumptions are same as in (A).

Two curves show that the oil-film thickness becomes very small before $M\beta$. The chain lines show the imaginary value of minimum thickness. In

the case of (B), $h_{\min}$ increases with moving of mating position in mating of two pairs of gear-teeth, and then it decreases with an approach to M'_γ. In mating of one pair of teeth, $h_{\min}$ becomes small due to supporting the total load. With an approach to M''_β, $h_{\min}$ increases and this increase continues to the range over M''_β. After this increase, $h_{\min}$ decreases with an approach to the ending of mating, and it shows a smaller value after M_γ than that before M_β.

5. Transient Characteristics of Oil-film on the Mating Gear-tooth Surface

5. 1. Experimental Equipment and Procedure

The variation of electrical resistance of oil-film between the mating teeth, which is measured by using ordinary gears, does not show the accurate variation of oil-film thickness, because, in mating of two pairs of teeth, two contact parts form a parallel resistance circuit[6]–[8]. In order to obtain accurate results, the following conditions must be satisfied in test gears:

(a) Test gears have the same function as ordinary gears.

(b) There is only one conductible part in the measuring circuit in overall range of mating of a tooth.

Fig. 29 shows the special test gear which is manufactured in order to satisfy the above conditions. As shown in the figure, this test gear consists
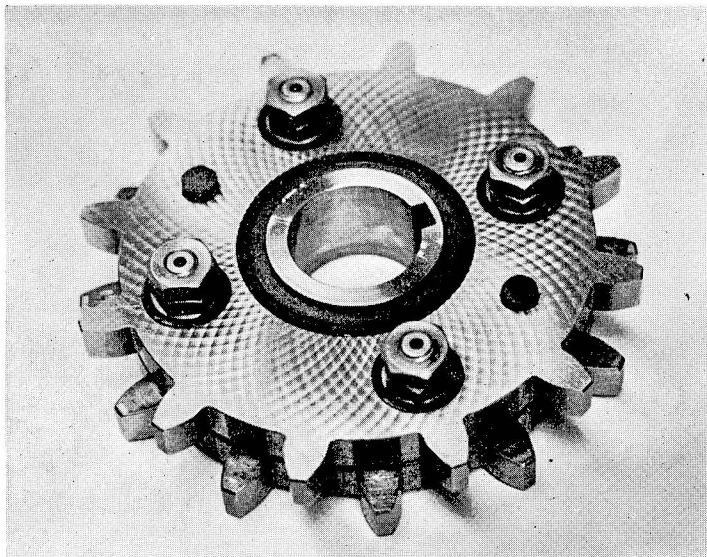

Fig. 29. Test gear.

of two tooth-lacked gears, and it is manufactured according to the following process.

(1) Manufacturing two ordinary gears which has an even number of teeth, and then removing the teeth alternately.

(2) Carburizing the tooth surface, and grinding both sides of gear blank and the inside- and the outside-diameters.

(3) Constructing two tooth-lacked gears between which an insulating disk is placed, and grinding the tooth surfaces.

Main dimensions of test gears are shown in Table 1. The error of

Table 1.

Tooth form	Involute standard tooth of ordinary depth
Diameter of pitch circle	120 mm
Module	5
Number of tooth	24
Pressure angle	20°
Contact width	10 mm
Gear ratio	1
Gear material	Ni–Cr–Mo Steel

normal pitch is less than 7μ in test gears used.

The experimental equipment used is shown in Fig. 30, and its main part has the same construction as the equipment shown in Fig. 10. One of the tooth-lacked gears is connected with the slip-ring ⑰ by a lead-wire
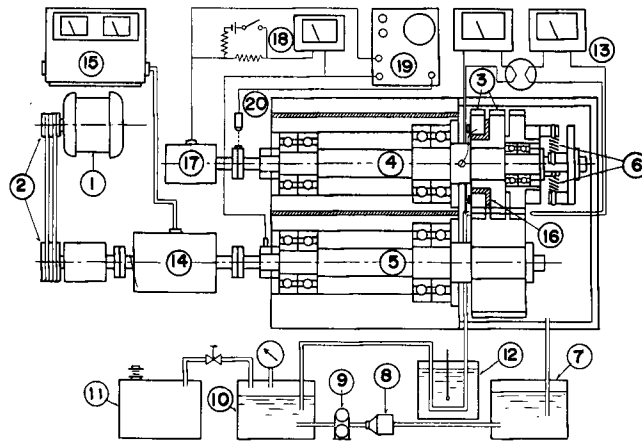

Fig. 30. Arrangement of experimental equipment.

through the hollow shaft ④.   The variation of oil-film thickness is observed by the oscilloscope ⑲ as voltage drop variation.   The mating position of the test gear is picked up by the photo-transistor ⑳.   The lubricating method for gears is the oil-jet lubrication.

5.2.   Experimental Results

Fig. 31 shows some oscilloscope traces of h_0 variation signals in mating

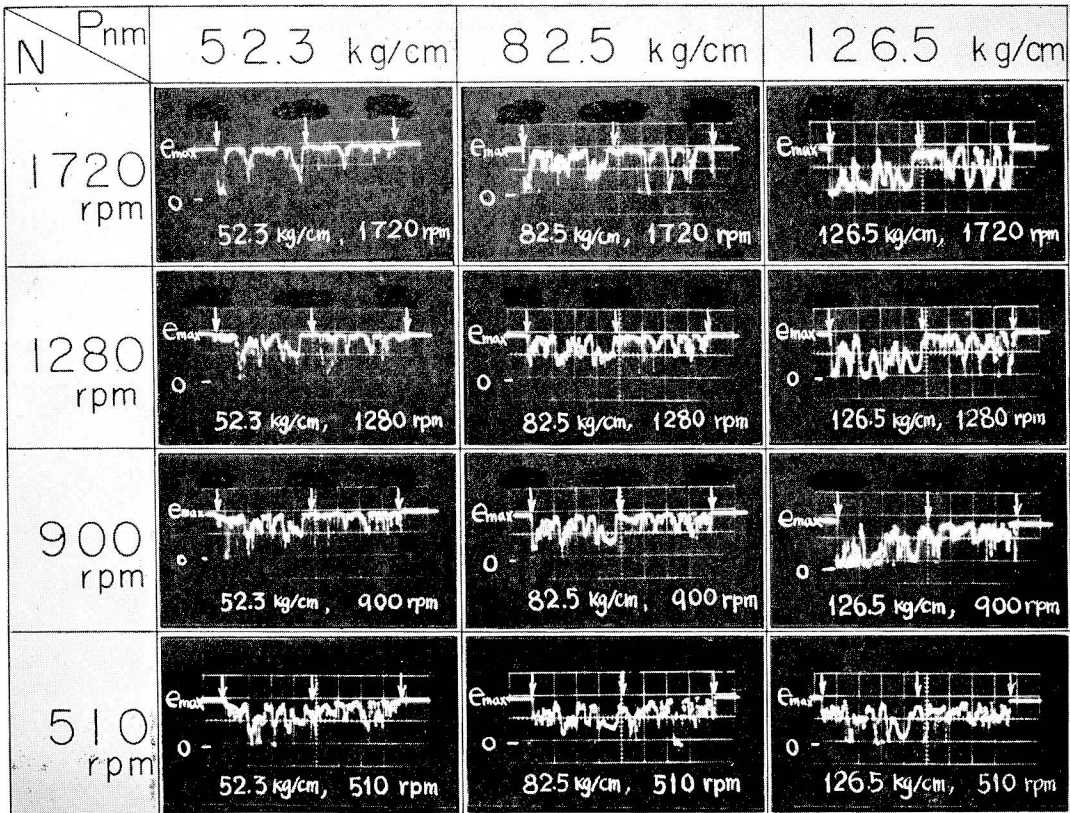Fig. 31.   Oscillograms of variation signals of oil-film thickness on mating gear-tooth surface.

gears, which are lubricated by straight turbine oil ♯90 ($\eta = 0.0042$ kg·s/m²). In the figure, maximum voltage drop $e_{\max}$ for $h_0 = \infty$ is 0.106 V, and three arrows show the mating position as follows: the beginning, the pitch and the ending points from the left to the right, respectively.   At the beginning of mating, the addendum part of the test gear is in mesh with the deddendum part of the other gear, because the test gear is the driven gear.   In the same procedure in Eq. (21), the mean normal load P_{nm} for this test gear is

obtained as follows:

$$P_{nm} = 0.62\, P_n$$

From the oscillograms, it is found that oil-film thickness has the minimum value at the beginning of mating through all the range of mating with exception of the case of low speed, and it increases with moving of mating position in mating of two pairs of gear-teeth. At the boundary changing from mating of one pair to two pairs of gear-teeth, oil-film thickness decreases, but it shows a steep increase with an approach to the pitch point and has the maximum value in the vicinity of the pitch point. In the succeeding mating of two pairs of teeth, oil-film thickness decreases with an approach to the ending of mating, but it has a greater value at the ending of mating than that at the beginning of mating.

These transient characteristics obtained experimentally are in a good agreement with the theoretical result as shown in Fig. 28, with exception that, in the experimental results, oil-film thickness has the minimum value at the beginning of mating and the maximum value in the vicinity of the pitch point.

It is thought that the former difference is caused by neglecting the action of the impact load at the beginning of mating, and the latter difference is caused by neglecting the variation of oil viscosity due to the increase of pressure and the decrease of sliding in the vicinity of the pitch point. By taking into consideration the influence of these factors upon the oil-film formation, a better result will be obtained from the dynamic lubrication theory.

Conclusion

The fundamental lubrication characteristics of rollers and gears were experimentally clarified, and it is deduced that the analysis of the dynamic lubrication phenomena is a very important problem in order to clarify the principle of oil-film formation in gears.

The theoretical result, calculated from the dynamic lubrication theory in consideration of the tooth deflection, showed particularly at the beginning part of mating a good agreement with the experimental results which were obtained by using a specially manufactured test gear. A better theoretical result will be obtained by taking into consideration the action of the dynamic load and the variation of oil viscosity in addition to the discontinuity of contact, the tooth deflection, the variation of load distribution and the variation of relative radius of curvature.

References

1) H. M. Martin : Engng., **102**, 191 (1916).
2) E. Buckingham : "Spur Gears", (1928).
3) H. E. Merritt : "Gears", (1946).
4) G. Niemann und H. Glaubitz : Z–VDI, **92**, 923 (1950).
5) H. Walker : Engr., 434 (1938).
6) T. B. Lane and J. R. Hughes : Brit. J. Appl. Phys., **3**, 315 (1952).
7) I. O. MacConochie and A. Cameron : Trans. ASME, **81**, 29 (1959).
8) D. W. Dareing and E. I. Radzimovsky : Trans ASME, **85**, 451 (1963).